AN ABSTRACT OF THE THESIS OF

Saroj Karki for the degree of Master of Science in Industrial Engineering presented on June 27, 2018

Title: Enabling Feasibility Assessment of Solar Thermal Energy Systems for Industrial Process Heating Applications

Abstract approved: _____

Karl R. Haapala Brian M. Fronk

Existing studies on industrial heat demand have shown that more than 50% of the industrial process heat demand is in the range of low (<60 °C), medium (60-150 °C), and medium-high (<250 °C) temperatures. Most of the manufacturing industries across the world depend on combustion of carbon-based fossil fuels, either partially or fully, for the generation of process heat. Commercially available solar thermal technologies are capable of generating a significant portion of low temperature process heat, which would reduce the use of fossil fuels, reducing the associated energy cost volatility and carbon emissions. Moreover, the improvement and proliferation of solar collector technology, and the introduction of solar-friendly policies in recent years have made solar thermal systems economically competitive investments with long-term, inflation-protected returns. Despite this tremendous benefit, the deployment of solar thermal systems for industrial process heating is surprisingly low.

The major barriers for the deployment of solar thermal energy systems for industrial process heating include a poor understanding of operational characteristics of solar thermal systems at different heating loads and insolation values, and a lack of robust

and cost-effective design decision support tools for appraising the merits of individual projects. The research presented herein aims to contribute in lowering the barrier for industrial scale deployment of solar thermal energy systems through: 1) Explanation of the characteristics performance of a solar flat-plate thermal system with backup gas heaters (a solar/gas hybrid heating system) at different heating loads and insolation values that approximate scaled process heating requirements of different industrial processes via an experimental study, 2) Identification of process heating temperatures that might be economically served with solar/gas hybrid heating systems based on site insolation characteristics, collector characteristics, and gas prices, 3) Identification of solar/gas hybrid heating system configurations that would provide higher system efficiency when combining solar and gas heating modes, and 4) Development and demonstration of design decision support tools for feasibility assessment of solar thermal energy systems. The outcomes of this research will enable engineers and industry decision-makers to analyze what-if scenarios to evaluate the feasibility of solar thermal systems for their applications based on site-specific data, while reducing cost and demand of technical resources required to perform the feasibility assessment.

Enabling Feasibility Assessment of Solar Thermal Systems for Industrial Process Heating Applications

by
Saroj Karki

A THESIS

submitted to

Oregon State University

in partial fulfillment of
the requirements for the
degree of

Master of Science

Presented June 27, 2018
Commencement June 2019

Master of Science thesis of Saroj Karki presented on June 27, 2018

APPROVED:

Co-Major Professor, representing Industrial Engineering

Co-Major Professor, representing Industrial Engineering

Head of the School of Mechanical, Industrial and Manufacturing Engineering

Dean of the Graduate School

I understand that my thesis will become part of the permanent collection of Oregon State University libraries. My signature below authorizes release of my thesis to any reader upon request.

Saroj Karki, Author

ACKNOWLEDGEMENTS

I would like to express my gratitude to my co-advisor Dr. Karl R. Haapala, representing my major in Industrial Engineering and option in Manufacturing Systems Engineering, for the unwavering support, guidance, motivation, and advice he has provided me throughout my time as a student. His technical and editorial advice was essential to completion of this thesis. Working with him truly affected my ethics, personality, and research attitude. Thank you for granting me the honor and opportunity of working under your supervision.

I must express my sincere gratitude to my co-advisor Dr. Brian M. Fronk, representing my major in Industrial Engineering and minor in Mechanical Engineering, for his patient guidance and encouragement in completion of this thesis. He continuously provided valuable feedback to my work and steered me in the right direction whenever he thought I needed it. It was fantastic to have the opportunity of working majority of my research in his lab.

This work would not have been possible without the financial support from the U.S. Department of Energy through the Energy Efficiency Center/Industrial Assessment Center at Oregon State University. I am especially indebted to Mr. Joseph F. Junker, Director of the OSU Energy Efficiency Center, for his immense support and guidance in the development of this work.

I would also like to acknowledge the other members of my graduate advisory committee: Dr. David Kim and Dr. Wade Marcum for serving on my committee.

Finally, I must express my very profound gratitude to my parents for providing me with unfailing support and continuous encouragement throughout my years of study and through the process of researching and writing this thesis. This accomplishment would not have been possible without them. Thank you.

CONTRIBUTION OF AUTHORS

Chapter 3: Manuscript 1

Dr. Brian M. Fronk assisted in this study in the form of developing the research idea and methods, and assistance in data analysis and manuscript writing. Dr. Karl R. Haapala provided input and direction of the work and helpful review and feedback.

Chapter 4: Manuscript 2

Dr. Karl R. Haapala assisted in this study in form of developing the research idea and methods, and assistance in manuscript writing, planning, management, and advice. Dr. Brian M. Fronk provided helpful review and feedback.

TABLE OF CONTENTS

Page

LIST OF FIGURES

Figure Page

LIST OF TABLES

Chapter 1. Introduction

1.1. Motivation

The industrial sector is the largest heat-consuming sector, accounting for approximately 43% of the total heat energy consumption globally [1]. Most of the manufacturing industries across the world depend on the combustion of carbon-based fossil fuels, either partially or fully, for generation of process heat [2]. Fossil fuels are limited and non-renewable, and their depletion has been identified as a future challenge [3]. Moreover, combustion of fossil fuels leads to serious environmental issues, such as air pollution, global warming, and acid rain. In contrast, renewable energy sources are inexhaustible with minimal associated global warming emissions [4]. Thus, renewable energy systems present an opportunity to reduce fuel consumption and carbon emissions.

Solar thermal technology providing industrial heating needs have been the subject of academic and commercial investigation for decades. Commercially-available solar thermal technologies can easily generate a significant portion of low temperature process heat [5], which would reduce the use of fossil fuels, reducing the associated energy cost volatility and carbon emissions. With the improvement and proliferation of solar collector technology, and with the introduction of solar-friendly policies in recent years, solar thermal systems are becoming economically competitive investments with long-term, inflation-protected returns [6]. In addition to the energy cost savings, job creation is another key economic benefit offered by solar thermal systems—an estimated 828,000 jobs in the field of production, installation, and maintenance of solar thermal systems were created worldwide in 2016 [7].

Despite the tremendous benefits, the actual deployment of solar thermal systems for industrial process heating is surprisingly low. An installed solar thermal capacity of only 456 GWth was recorded worldwide at the end of 2016. Of this, industrial process heating accounted for only around 3% of the total installed capacity [8]. Thus, further work is required to identify and address the barriers that are impeding the dissemination of solar thermal systems for industrial process heating applications.

1.2. Background

Solar thermal systems are a mature technology and have been commercialized across the world. Application of solar thermal systems for domestic water heating is the most established technology, with a proven record of performance worldwide [9]. With the increasing environmental concerns and the energy cost volatility associated with the use of carbon-based fossil fuels, it is potentially advantageous to expand the use of solar thermal systems for industrial process heating applications. Compared to the domestic sector, the industrial sector has a wider range of applications where solar thermal systems can be easily integrated. Existing studies [10–13] on industrial heating demand have shown that more than 50% of industrial process heat demand is in the range of low (< 60 °C), medium (60 to 150 °C), and medium-high (< 250 °C) temperatures. The highest demand for low temperature process heat come from small and medium manufacturing industries, such as food and beverage, dairy, paper, textile, and wood industries [10,11,14,15], making them the most promising sectors for application of solar thermal energy systems. The most relevant manufacturing processes that use low temperature heat are washing and cleaning, sterilization, pasteurization, concentration, water heating, drying, and pre-heating [2]. Another advantage of using solar thermal systems in the industrial sector is that industrial loads are often uniform throughout the year and coincide with solar hours, which results in better performance of solar energy collectors [12]. Despite this potential, the deployment of solar thermal systems for industrial process heating remains low [16].

A major barrier for deployment of solar thermal systems for industrial process heating applications is the poor understanding of operational characteristics of the system at different heating loads and site insolation values. The most well-known drawback of solar thermal system is that solar energy is intermittent—solar energy is only available during day time and is geography and weather dependent. Due to the diurnal and seasonal variation of available solar energy, an auxiliary heating source is generally necessary to provide backup heating whenever solar energy fails to meet the energy demand. Direct-fired burners powered by natural gas are the most commonly used heating systems for generating process heat in manufacturing industries [17].

Therefore, for industrial process heating applications, most solar thermal energy systems would likely rely on natural gas fired backup heating systems for reliability (also known as a solar/gas hybrid heating systems). In the United States, another reason for using natural gas-fired heaters is that the cost of natural gas is below the cost of electricity on a kWh-to-kWh basis [18]. Furthermore, depending on the feedstock energy source for generating electricity (e.g., from wind versus coal), there may be advantages from carbon emissions and primary energy consumption perspectives in obtaining auxiliary heating directly with gas [19]. In a real application, the general practice is that solar energy is first used to heat process fluids to a highest possible temperature, and if the solar energy is not sufficient, then gas energy is used to accomplish the final lift. However, previous studies [20,21] have shown that gas-fired heaters are inherently less efficient when heating high temperature fluids. Therefore, lower overall system efficiency than expected may be observed while operating a solar collector in conjunction with a gas-fired heater. Since this efficiency varies depending on the amount of pre-heating provided by solar input, it is challenging to accurately predict the actual cost and energy savings offered by solar/gas hybrid heating systems. This characteristic performance of solar/gas hybrid systems is often misunderstood.

Another major barrier for the deployment of solar thermal systems for industrial process heating applications is the lack of suitable design guidelines and tools required for appraising the merits of individual projects [16]. Business owners will want to invest in solar thermal systems only if there is a clear benefit. However, they often do not have the capacity (money or expertise) to do the feasibility assessment themselves. A lot of times, independent consultancies are hired to do the assessment. That, however, comes at a cost not many business owners may be willing to invest in. A few studies in the past [10,11,22–24] have assessed the practicality of solar thermal energy systems for industrial process heating applications, but those studies are industry and location specific and cannot be used as a general design guideline. Moreover, those studies were performed using simulation-based design decision support tools. Such tools are costly, require higher computational power, and require technical experience to operate, which small and medium manufacturing companies often lack. The possibility of waste heat recovery is an important aspect to be considered while designing and assessing the

feasibility of solar thermal systems [25], which existing design decision support tools do not account for. There is a dearth of simplified and cost-effective design decision support tools reported in the literature that have addressed the above-mentioned limitations in their cost and energy calculation models.

1.3. Problem Statement

Poor understanding of the operational characteristics of solar thermal systems and a lack of robust and cost-effective design decision support tools for appraising the merits of individual projects has hindered the deployment of solar thermal systems for industrial process heating applications. The requirement of cost and technical expertise to conduct feasibility assessments has made industry decision makers reluctant towards analyzing the possibility of solar thermal in their businesses.

1.4. Research Objectives

The overarching goal of this research is to lower the barrier for industrial scale-deployment of solar thermal energy systems by providing a better design decision guidance. To achieve this goal, the following research objectives are pursued within this thesis:

Objective 1: Investigate the operational characteristics of a solar/gas hybrid thermal energy system at different heating loads and insolation values that approximate scaled process heating requirements of different industrial processes. Identify process heating temperatures that might be economically served with solar/gas hybrid heating systems based on site insolation characteristics, collector characteristics, and gas prices.

Objective 2: Identify a solar/gas hybrid heating system configuration that would provide optimal system efficiency when operating the system in a combined solar and gas heating mode.

Objective 3: Assist industry analysts in evaluating the feasibility of solar thermal energy systems with gas-fired back up heaters by providing an easy to use design decision support tool.

This research will focus specifically on flat-plate solar collectors.

1.5. Research Tasks

To fulfill the research objectives, the following research tasks are undertaken:

Task 1: Perform a set of designed experiments of a solar/gas hybrid domestic water heating system under different modes of heating, temperature lifts, and solar insolation values. Subtasks include calculating a) solar collector efficiency, b) gas-fired heater efficiency, and c) solar/gas combined system efficiency values using the collected data.

Task 2: Develop a design decision support tool to assist industry analysts in evaluating the feasibility of solar flat-plate collector energy systems in their businesses. Subtasks include a) reviewing existing solar thermal performance prediction models in the literature and identifying appropriate models, b) developing cost model and collecting information to support cost analysis, c) documenting thermal performance prediction and cost calculation model in a spreadsheet.

The use of the decision support tool along with the analysis of several what-if scenarios are demonstrated through an example application.

1.6. Thesis Outline

Chapter 1 provides motivation and background for this research, along with a problem statement and research tasks.

Chapter 2 provides the background on solar thermal energy systems and presents a review of existing literature on experimental investigation of solar flat-plate collectors, potential of solar heat for industrial processes, and analysis of solar thermal systems for industrial process heating.

Chapter 3 is a journal article titled, “Investigation of a Solar/Gas Hybrid Water Heating System Combined System Efficiency.” This article summarizes the results obtained from the experimental study of solar/gas hybrid water heating system under different temperature lifts and local insolation values.

Chapter 4 is a journal article titled, “Technical and Economic Feasibility Assessment of Solar Thermal Energy Systems for Small and Medium Manufacturing Enterprises.”

This article proposes a methodology to assess the technical and economic feasibility of solar flat-plate collector energy systems.

Chapter 5 summarizes and concludes the research presented in the previous section. It also identifies the specific contributions of this research and opportunities for future work.

Chapter 2. Literature Review

Solar thermal systems are a simple and cost-effective renewable energy technology for harnessing the sun's energy to generate thermal energy. A solar thermal system typically consists of solar energy collectors, a heat exchanger, an energy storage tank, and a control system. Solar collectors capture the incident solar radiation and transfer it to a working fluid flowing inside the collector tubes. The energy carried by the working fluid is either used directly, or used to charge a thermal energy storage tank. Because of the diurnal and seasonal variation of solar energy, an auxiliary energy source is used in conjunction with solar collectors to provide the backup heating whenever the solar energy falls short.

A flat-plate collector (FPC) is the most common type of solar collector appropriate for harvesting solar energy at low fluid temperatures (30 to 80 °C) [26]. As shown in Figure 2.1, a FPC consists of: a metal box with a transparent glass or plastic cover (glazing) that reduces heat loss from the top, a dark-colored flat-plate absorber on the bottom, and collector tubes filled with heat transfer fluids [27]. The underside of absorber and sides of the metal box are well insulated to minimize heat loss [27].

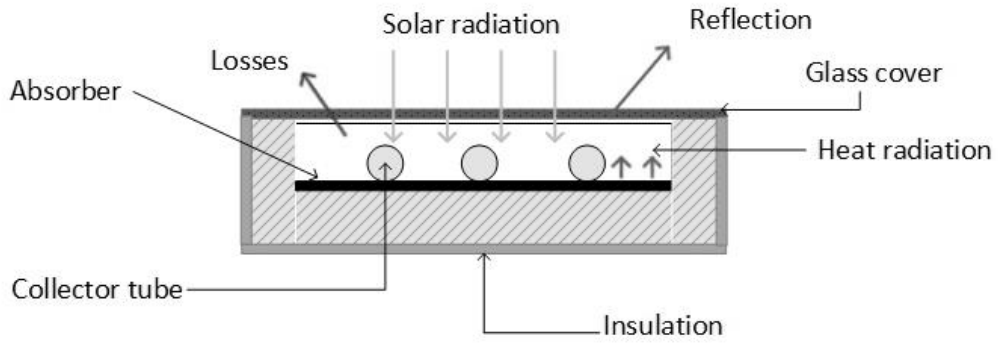

Figure 2.1: Sketch of a solar flat-plate collector

Collector glazing is made up of glass or other similar radiation-transmitting materials because of their high transmissivity of short-wave radiation and low transmissivity of long-wave radiation [27]. Glass with low-iron content has been widely used as the glazing material [27] because of its high transmittance of solar radiation (approximately 0.82-0.87 at normal incidence [28]) and an essentially zero transmittance for long-wave thermal radiation (5.0 μm – 50 μm). The collector absorber plate is the heart of the

FPC. It absorbs the maximum possible radiation incident through the glazing [27]. The thermal performance of an absorber plate depends on its material properties and design parameters [29].

As reported by Duffie and Beckman [26], for steady state operating conditions, the rate of useful energy collected by a solar FPC can be calculated using the Hottel-Whillier-Bliss equation as (Eq. 2.1):

$$q_{useful} = F_R A_C [I_T(\tau\alpha) - U_L(T_i - T_a)]^+ \quad (2.1)$$

where F_R is the collector heat removal factor, A_C is the collector aperture area value, I_T is the average daily solar radiation, U_L is the collector overall heat loss coefficient, T_i is the collector fluid inlet temperature, T_a is the ambient temperature, and $\tau\alpha$ is the product of collector transmittance and absorptance.

The collector efficiency (η) is the ratio of the useful thermal energy delivered by the collector to the usable solar irradiance falling on the collector's aperture area and is expressed as [30] (Eq. 2.2):

$$\eta = \eta_o - k_1 \frac{(T_i - T_a)}{I} - k_2 \frac{(T_i - T_a)^2}{I} \quad (2.2)$$

where η_o is the efficiency when $T_i = T_a$, and k_1 and k_1 are the collector heat loss coefficient values.

2.1. Experimental Investigation of Solar Flat-Plate Collectors

Several standard test procedures have been developed for testing and rating solar collectors under steady state and quasi-dynamic test conditions. The most commonly used test standards are ASHRAE 93-2003 [31] and EN 12975-2 [32]. Numerous experimental studies have been carried out to measure the efficiency of solar FPCs following standard test conditions. Anderson et al. [33] performed experiment-based study to calculate the thermal performance of a 3.45 m^2 commercial FPC using ASHRAE 93 standards and found: collector heat removal factor value, $F_R U_L$ of 4.25 W

m^{-2} K^{-1}, maximum collector efficiency value (η_o) of 75.2%, and collector heat loss coefficient values, k_1 and k_1 equal to 3.046 and 0.01989, respectively.

Rojas et al. [34] performed experiment and simulation-based study of solar FPCs following ASHRAE 93-2003 and EN 12975-2 standards and found that the collector thermal parameters, $F_R U_L$ and $F_R(\tau\alpha)$ obtained by the two test methods showed good agreement. Zambolin and Del Col [35] and Osório & Carvalho [36] experimentally measured the thermal efficiency of solar FPC under steady-state and quasi-dynamic conditions following EN 12975-2 standards.

However, these standards require experimental data to be collected under prescribed environmental conditions which may not necessarily represent the actual operating conditions experienced by the solar collectors. For example, a minimum solar radiation of 790 and 700 W m^{-2} is required by the ASHRAE 93 and EN 12975-2 standards, respectively, to conduct the thermal efficiency tests [34]. In practice, however, solar radiation values fluctuate depending on the climate conditions and time of the day. Furthermore, these standards are a test of the solar collector efficiency only, and do not account for the efficiency of an auxiliary heating system that would be required in many climate regions.

Some researchers have performed experimental studies of FPCs under real weather conditions. Ayompe and Duffy [37] studied the thermal performance of a commercially available forced circulation solar water heating system with a 4 m^2 FPC array and a 300 L storage tank in Dublin, Ireland. They monitored the thermal performance of the system for a period of one year and found collector efficiency and overall system efficiency values of 45.6% and 37.8%, respectively. Michaelides and Eleftheriou [38] conducted an experimental study of a domestic solar water heating system with a 3 m^2 flat plate collector and a 68 L storage tank. They monitored the system for a period of two years under real weather conditions in Cyprus and found that the annual average daily performance of the system was relatively insensitive to solar radiation fluctuations ranging from 800 to 1100 W m^{-2}. The effect of fluctuating solar radiation was pronounced only in the instantaneous energy and efficiency values.

Rodriguez-Hidalgo et al. [39] studied the thermal performance of a 50 m^2 FPC array located in an experimental solar facility in Madrid, Spain. Experimental data were recorded for an entire year at 10-minute intervals, and collected data were used to quantify the collector thermal efficiency drop caused by: wind thermal loss, collector aging, thermal capacitance, incident angle of irradiation, and radiation losses. The most significant collector thermal efficiency drops were due to wind loss (15.7%) and collector surface aging (15%). Other collector thermal efficiency drops were: 7.6% drop due to variable incident angle of irradiation, 3.2% drop due to variation in thermal capacitance, and 1.3% drop due to external radiation losses.

2.2. Potential of Solar Heat for Industrial Processes

While more limited than investigation of domestic heating, several studies have analyzed the potential of solar industrial process heating for different countries. Schweiger et al. [11] determined the potential of solar thermal systems for low (<60 °C) and medium-low (60-150 °C) temperature applications in Spain and Portugal. Their study found that the highest demand for low temperature heat came from the food and beverage industry, making it the most promising manufacturing sector for application of solar thermal systems. Other suitable manufacturing sectors were identified as chemicals, textiles, paper, and leather industries. Vannoni et al. [40] investigated the potential of solar thermal systems in Greece, Belgium, and a few manufacturing sectors in Germany. Their study identified chemicals, food and beverage, paper, textiles and tobacco industries as the most suitable manufacturing sectors for the application of solar thermal systems.

Kalogirou [10] performed a simulation-based study to investigate the potential of solar thermal systems for industrial process heating applications in Cyprus. He identified the food and beverage industry as the most promising manufacturing sector for the application of solar thermal systems. He further suggested that washing and drying processes in general are suitable for the application of solar heat. Vannoni et al. [15] studied the potential of solar thermal systems for industrial process heating applications in Italy. The available roof and facade area was considered as a design constraint in their study. They concluded that around 3.7% of the industrial heat demand in Italy

could be met by solar thermal systems and they mentioned chemicals, food and beverage, motor vehicles, paper, textiles, tobacco and leather industries as the most suitable manufacturing sectors for application of solar thermal systems.

In the context of the US, a study [41] on the potential of renewable energy technology for industrial process heating showed that depending on the specific industry, process heating applications accounted for between 35% and 50% of the total energy consumption, which can be met by renewable energy technologies. The study further suggested that manufacturing process such as water heating, cooking, pressurization, sterilization, and bleaching are well-suited for application of solar thermal systems.

Kurup and Turchi [42] studied the potential of solar thermal systems for industrial process heating in California, US. Their study focused on food, paper, petroleum, chemicals, and primary metals manufacturing industries. They compared the cost of energy from solar-thermal collectors with the cost of energy from natural gas in California, and concluded that solar industrial process heating systems can be cost-effective, even when the price of natural gas is low. They further recommended to identify pilot projects to promote deployment of solar process heating systems.

2.3. Analysis of Solar Thermal Systems for Industrial Process Heating

Regarding the feasibility analysis of solar thermal energy systems for industrial process heating applications, some studies have been performed in the past for different countries or climate regions. Kalogirou [10] analyzed the viability of a number of solar collector technologies with respect to life-cycle cost savings and energy yield for industrial process heating applications in Nicosia, Cyprus. Using TRNSYS (TRNSYS, the Transient System Simulation Tool [43], is one of the most commonly used software packages to simulate the behavior of solar thermal systems) simulations, a range of annual average energy collection of 550 to 1100 kWh m-2 was obtained for an industrial application where 2000 kg hr^{-1} of hot water was needed in a temperature range of 60 to 240 °C.

Schweiger et al. [11] performed a simulation-based study to estimate annual collector yields for a variety of solar process heat applications in Spain and Portugal. Their study

concluded that the size limitation of solar collectors in most cases is due to the available roof and ground area. They also concluded that the decision for implementation of solar thermal systems is mainly driven by the actual cost savings offered over the lifetime.

Aidonis et al. [14] presented design guidelines for solar thermal plants in industrial heating. They stated that for industrial processes to be suitable for integration of solar thermal systems, the thermal loads should last for at least 75% of the time throughout the year and must include summer months. They recommended that a solar fraction range of 10 to 50% would be feasible based on the space restrictions for collector installation and the total system installation cost. Additionally, they recommended using a rule of thumb of 50 L m^{-2} collector area to dimension the storage tank.

Benz et al. [44] performed TRNSYS simulations to design a solar thermal system for a bottle washing machine in a brewery and for a spray dryer in a dairy in Germany. Their study found that the efficiency of solar collectors for industrial process heating is comparable to the efficiency of solar collectors for domestic water heating. Eskin [45] performed experimental and simulation-based studies of a solar process heating system at a textile plant in Turkey. Cotrado et al. [22] performed simulations to predict the lifetime performance of a solar process heating system in a meat plant in Austria. They found that the solar thermal system provided approximately 475 MWh heat annually.

El Mkadmi and Wahed [23] performed TRNSYS simulations to study the performance of solar thermal systems in a dairy industry under three different climatic conditions: Cyprus, France, and Morocco. The average daily heat demand was assumed to be 277 kWh. Their study found that 89%, 76%, and 94% of the total heating load was met by a solar thermal system for Cyprus, France, and Morocco, respectively.

2.4. Synthesis and Contribution

A review of existing literature on the experimental study of solar FPCs (shown in Table 2.1) found that most existing studies are based on solar FPCs with an electric immersion heater as the auxiliary energy source.

Table 2.1: Summary of existing experimental studies on solar FPCs.

Author	Type of Study	Findings	Limitations
Rojas et al. [34]	Efficiency investigation of solar FPCs following ASHRAE 93-2003 and EN 12975-2 standards	Collector thermal parameters, $F_R U_L$ and $F_R(\tau\alpha)$ obtained by the two test methods showed good agreement	- Data obtained from standard test methods do not necessarily represent real life operating conditions - Did not account for efficiency of backup heating systems
Zambolin and Del Col [35]	Efficiency investigation of a solar FPC under quasi-dynamic conditions following EN 12975-2 standards	Reported collector efficiency, annual average energy collection, and collector thermal losses values	- Data obtained do not necessarily represent real life operating conditions - Did not account for efficiency of backup heating systems
Ayompe and Duffy [37]	Efficiency study of a domestic solar FPC under real weather conditions	Reported collector efficiency, annual energy collection, and collector losses values	- Collector efficiency was calculated for only a single heating load (20 °C to 60 °C) - Experimental study used electric resistance backup heating system. It did not consider gas-fired backup heaters.
Rodriguez-Hidalgo et al. [39]	Efficiency study of a 9-year load solar FPC under real weather conditions	Quantified thermal efficiency drops: 15.7% efficiency drop was due to wind loss and 15% was due to collector surface aging	- Experimental study used electric resistance back up heating system. It did not consider gas-fired backup heaters.

Electric resistance heaters are 100% efficient [46], meaning all the input electric energy is converted into heat and supplied to the load. This conversion efficiency is not dependent on the temperature of the heated load. Since the efficiency of electric heating is constant, it is straightforward to predict the cost and energy of the required auxiliary energy when the solar fraction is known.

Unfortunately, electric resistance auxiliary heating systems are uncommon in solar industrial process heating applications. Since direct-fired gas burners are the most commonly used heating systems for process heat generation in manufacturing industries, most industrial solar thermal process heating systems would likely implement natural gas fired heaters for auxiliary heating (a solar/gas hybrid system). However, previous studies [20,21] have shown that gas-fired heating systems are inherently less efficient when heating high temperature fluids. With gas-fired heating systems, the input to load conversion efficiency varies depending on the amount of heat transferred in the heat exchanger, which is directly impacted by the temperature difference between the cold fluid (combustion gases) and the hot fluid (process fluid).

In a solar/gas hybrid heating system where the solar collector is used in conjunction with a gas-fired heater, the partial heating of process fluid provided by solar input reduces the log-mean temperature difference (LMTD) value for the gas heater, reducing the efficiency of the gas burner. Therefore, lower overall system efficiency than expected may be observed while running a solar/gas hybrid heating system in a combined solar and gas mode. Since this efficiency varies depending on the amount of pre-heating provided by the solar input, it is challenging to accurately predict the actual cost and energy savings offered by a solar/gas water heater. To accurately appraise the merits of solar thermal systems, it is necessary to reflect the effect of this efficiency variation in cost and energy savings calculation models.

Research studies reported in the literature have not addressed this efficiency variation issue caused in a solar/gas hybrid system while running in a combined solar and gas mode. Thus, to address this deficiency, a set of designed experiments were performed at Oregon State University. The thermal performance of a commercial solar/gas water hybrid water heating system with a 6.44 m^2 flat plate solar collector array and a 22.3 kW natural gas burner were measured under different modes of heating, temperature lifts, and solar insolation values. The system was operated under three different modes of heating: solar only, gas only, and combined solar/gas mode. Using the collected data, the efficiency value for each mode was calculated and is reported in Chapter 3 of this thesis. The efficiency reduction trend of gas-fired heating system when operating in

conjunction with solar collectors was calculated and is also reported in Chapter 3. Based on the experimental efficiency results, a potential configuration of solar/gas hybrid system that would provide optimal efficiency for the combined solar and gas mode of heating is suggested.

A review of existing literature on solar thermal for industrial process heating showed that solar thermal energy systems can economically provide low temperature industrial process heat, while providing external benefits such as reduced reliance on fossil fuels and reduced emissions. Hence, manufacturing industries should start making informed decisions on the deployment of solar thermal technologies in their businesses. However, there is lack of reliable site-specific information required for appraising the merits of individual projects. Some studies in the past have analyzed the economic feasibility and long-term performance of solar industrial process heating systems. Those analyses, however, are industry-specific and are not applicable as a general design guideline.

Further, most of the existing feasibility assessment tools are simulation-based. Such simulation-based tools are expensive, require computational speed, and most importantly, require significant technical knowledge to operate. As mentioned-before, most of these tools often do not account for efficiency variation of back up gas heating system that occurs when operated in conjunction with solar collectors. Another limitation of existing feasibility assessment tools is that such tools, in their cost calculation model, do not consider the possibility of waste heat recovery options that might occur within an industrial facility. Hence, there is a need for a robust and cost-effective decision support tools to help industry analysts quickly and accurately design and assess the feasibility of solar thermal energy system in their businesses.

To address this issue, a simplified and cost-effective design decision support tool to assist industry analysts in evaluating the feasibility of solar flat-plate collector energy systems for industrial process heating was developed and is presented in Chapter 4 of this thesis. The tool allows for several what-if scenarios analyses that can be explored to identify feasible solar thermal system designs. A cost calculation model is developed, which enables the identification of a combination of solar flat-plate

collectors, a natural gas heating system, and a waste-recovery preheating system with lowest possible total cost. A sensitivity analysis is imbedded within the tool, which enables the quantification of uncertainties associated with input factors on the savings to investment ratio (SIR). An example application is presented to demonstrate the application of the tool.

CHAPTER THREE: INVESTIGATION OF COMBINED EFFICIENCY FOR A SOLAR/GAS HYBRID WATER HEATING SYSTEM

By

Saroj Karki, Brian M. Fronk, and Karl R. Haapala

To be submitted to the *Applied Thermal Engineering*

https://www.journals.elsevier.com/applied-thermal-engineering

Chapter 3. Investigation of Combined Efficiency for a Solar/Gas Hybrid Water Heating System

3.1. Abstract

In climate regions with large seasonal variations in solar radiation, such as the Pacific Northwest, a solar energy collector might not economically satisfy year-round domestic water heating demands, requiring an auxiliary unit, such as a natural gas-fired water heater. Previous studies have shown that the burner efficiency of a gas-fired water heater varies depending on the log-mean temperature difference between the cold fluid (water) and hot fluid (combustion gases). In a solar/gas hybrid water heating system where the solar collector is used in conjunction with a gas-fired heater, the partial heating of water provided by solar input reduces the log-mean temperature difference value for the gas heater, reducing the efficiency of the gas burner. Since this efficiency reduction varies depending on the amount of pre-heating provided by solar energy input, it is difficult to accurately predict the actual cost and energy savings offered by a solar/gas hybrid water heater. Hence, to predict the actual energy and cost savings under various design conditions, the performance of solar/gas hybrid systems must be better understood.

The purpose of this work is to experimentally determine the thermal performance of a solar/gas water hybrid water heating system with a 6.44 m^2 flat plate solar collector array and a 22.3 kW natural gas burner in Corvallis, Oregon. Under different temperature lifts and solar insolation values, the system was operated at three different modes of heating: solar, gas, and combined solar/gas mode. The overall system thermal efficiency value for each mode is calculated. The efficiency of the collector heating system was found to be 41.97%, 39.82%, and 35.05% at starting water temperature of 20, 30, and 51.5 °C, respectively. For starting water temperatures of 20, 30, and 51.5 °C, the efficiency of gas burner was found to be 69.2%, 66.4%, and 65.5% at the HHV and 76.7%, 73.6%, and 72.6% at the LHV of natural gas, respectively. In the combined solar/gas heating mode, the efficiency of the gas burner decreased with increasing solar fraction. For solar fractions of 4.93%, 9.40%, 11.39%, and 14.27%, the efficiency of the gas burner in terms of the HHV of natural gas was found to be of

69.08%, 66.80%, 66.17%, and 65.18%, respectively. Based on the experimental results, a configuration that would provide higher overall system efficiency for combined solar/gas heating is suggested.

3.2. Introduction

Water heating accounts for approximately 18% of the total residential energy consumption in the United States [47]. Historically and currently, the water heater market in the US has been dominated by traditional gas-fired and electric resistance storage type and tankless water heaters [48]. A breakdown of US residential water heating energy use indicates that approximately 48% of households use natural gas, while approximately 45% use electricity for water heating [49]. With the increasing concerns of carbon emissions and other environmental impacts associated with the extraction and use of fossil fuels, there is interest in developing renewable energy sources for domestic water heating.

Solar water heating systems (SWHS) are a simple and cost-effective renewable technology for harnessing the sun's energy to generate hot water. The main components of a typical SWHS are a solar collector, a hot water storage tank, and a control system. The operating principle is that the solar collector absorbs the incident solar radiation and transfers the energy to a working fluid (water or solar fluid) flowing inside the collector tubes. The heated working fluid can be used either directly in the form of hot water, or to charge a thermal energy storage tank from where energy can be drawn for use later. A flat-plate collector (FPC) is the most common type of solar collector used for harvesting solar energy at relatively low fluid temperatures [26], and has seen commercial application around the world. It consists of a selective flat plate absorber covered by a transparent glass or plastic cover (glazing) to reduce heat loss from the top surface, tubes to circulate the heat transfer fluid within the body of the collector, and insulation to minimize heat losses from the sides and bottom surface of the absorber plate [26].

The percentage of water heating energy required by a household that is provided by the solar collectors is quantified in terms of solar fraction. For a given collector area, solar fraction varies primarily with the amount of incident solar radiation [30]. Due to the

diurnal and seasonal variation of available solar energy, an auxiliary heating source is generally necessary to provide backup heating whenever solar energy fails to meet the energy demand [26]. Electric resistance heaters are the most commonly used backup energy source.

Numerous experimental studies have been carried out over the years to analyze the thermal performance of FPC solar water heating systems under steady-state and quasi-dynamic test conditions following EN 12975-2 [32] and ASHRAE 93-2003 [31] standards, among others. For example, Rojas et al. [34] and Anderson et al. [33] studied the thermal performance of FPCs under steady-state conditions following the ASHRAE standard, while Zambolin and Del Col [35] and Rodriguez-Hidalgo et al. [50] measured the thermal efficiency of FPCs under steady-stated and quasi-dynamic state following the EN standard. However, these standards require experimental data to be collected under prescribed environmental conditions which may not necessarily represent the actual operating conditions experienced by the solar collectors. For example, a minimum solar radiation of 790 and 700 W m^{-2} is required by the ASHRAE 93 and EN 12975-2 standards, respectively, to conduct the thermal efficiency tests [34]. In practice, however, solar radiation values fluctuate depending on the climate conditions and time of the day. Further, these standards are a test of the solar collector efficiency only, and do not account for the efficiency of an auxiliary heating system that would be required in many climate regions. Some researchers have performed experimental studies of FPCs under real weather conditions. Rodriguez-Hidalgo et al. [39] carried out an experimental study to evaluate the performance of a 50 m^2 FPC for domestic hot water heating and cooling application in Madrid, Spain. Using the collected data, they quantified the sensitivity of instantaneous thermal performance of solar collectors to the following factors: wind thermal loss, collector aging, thermal capacitance, irradiance incidence angle, and radiation loss.

Michaelides and Eleftheriou [51] studied the thermal performance of a solar water heating system utilizing a 3 m^2 FPC and 68 L storage tank under real weather conditions in Cyprus over a two-year period, and found that the annual average daily performance of the system was relatively insensitive to solar radiation fluctuations ranging from 800

to 1100 W m^{-2}. The effect of fluctuating solar radiation was pronounced only in the instantaneous energy and efficiency values. Ayompe and Duffy [37] experimentally measured the thermal performance of a solar water heating system with 4 m^2 FPCs located in Dublin, Ireland and reported an annual average daily solar fraction of 32.2%, collector efficiency of 45.6%, and overall system efficiency of 37.8%. In all above-mentioned studies, an electric immersion heater was used as the auxiliary energy source. Electric resistance heaters are 100% efficient [46], meaning all the input electric energy is converted into heat and supplied to the water. This conversion efficiency is not dependent on the temperature of the heated water. Since the efficiency of electric heating is constant, it is straightforward to predict the cost and energy of the required auxiliary energy when the solar fraction is known. However, with natural gas-fired water heating systems, the efficiency varies depending on the amount of heat transferred in the heat exchanger, which is directly impacted by the temperature difference between cold fluid (water) and hot fluid (combustion gases).

Presently, the cost of natural gas in the US is below the cost of electricity on a kWh-to-kWh basis [18], making natural gas backup an attractive option in terms of auxiliary energy cost. Furthermore, depending on the feedstock energy source for generating electricity, there may be advantages from carbon emissions and primary energy consumption perspectives in obtaining auxiliary heating directly with gas [19]. However, previous studies [21,52,53] have shown that efficiency of gas-fired water heaters decreases with increasing inlet water temperature. With an increase in inlet water temperature, the temperature driving force between the combustion gases and tank water decreases, reducing the heat transfer rate. In a solar/gas hybrid water heating system where the solar collector is used in conjunction with a gas-fired heater, the partial heating of process fluid provided by solar input reduces the log-mean temperature difference (LMTD) value for the gas heater, reducing the efficiency of the gas burner. Therefore, lower overall system efficiency than expected may be observed while running a solar/gas hybrid water heating system in a combined solar/gas mode. Since this efficiency varies depending on the amount of pre-heating provided by solar input, it is challenging to accurately predict the actual cost and energy savings offered by a solar/gas water heater.

Hence, to predict the actual energy and cost savings under various design conditions, the performance of solar/gas hybrid systems must be better understood. The objective of this work is to experimentally determine the thermal performance of a commercial solar/gas water hybrid water heating system with a 6.44 m^2 flat plate solar collector array and a 22.3 kW natural gas burner under actual operating conditions. The system was operated at three different modes of heating: solar only, gas only, and combined solar/gas modes for different temperature lifts and solar insolation values. Efficiency values for each mode were calculated. Based on the experimental efficiency results, potential configurations that would provide optimal efficiency for the combined solar/gas mode of heating are suggested.

3.3. Experimental Setup and Data Reduction Methods

3.3.1. Experimental Setup

An active closed loop hybrid solar thermal water heating system (STWHS) installed on a campus building at Oregon State University in Corvallis, Oregon (44.56° N, 123.27° W), provides the basis for this experimental study. The STWHS consists of 6.44 m^2 FPC array, a 265 L hot water storage tank, a pump with maximum flow rate of 0.63 L/sec, and a commercial control unit.

The collector array consists of three Schüco Slim V Plus FPCs connected in series; each FPC has a gross area of 2.32 m^2 and an aperture area of 2.148 m^2. The collectors face south and are inclined at 45 degrees. As stated by the manufacturer, each collector has an optical efficiency, or "zero loss efficiency," rating of 76.7%. The collector heat loss coefficient values, k_1 and k_2, are defined to be 3.71 and 0.016 $W\,m^{-2}\,K^{-1}$, respectively. The absorber plate is made up of copper tubes covered with a high selectivity coating that has short-wave absorptivity of 95% and long wave emissivity of 5%. Each collector is covered by a 4-mm thick low iron glazing of 91% transmittance. The sides and bottom surface of the collectors are insulated with mineral wool insulation (20 mm thick). The maximum operating temperature and pressure of the collectors are 120 °C and 10 bars, respectively.

The storage tank is a Schüco S WW 70-1GPN model, made up of stainless steel. It is equipped with an auxiliary 22.27 kW natural gas burner, which has a specified efficiency rating of 80% at lower heating value. The tank contains an immersed solar heating coil that allows heat transfer between the solar fluid and potable water. The solar coil has heat transfer surface area of 1.31 m^2. Non-CFC foam insulation (50.8 mm thickness) covers the sides and the top of the tank.

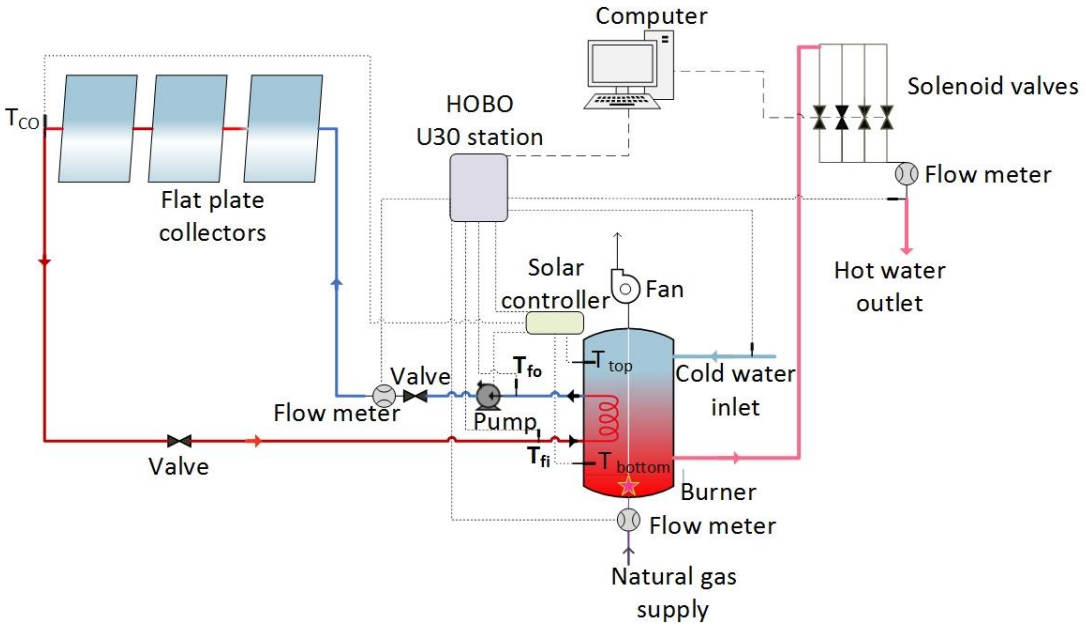

Figure 3.1: Schematic diagram of the experimental setup

A schematic diagram of the experimental setup is reported in Figure 3.1. A solution of water and propylene glycol (40% propylene glycol by mass) is used as the heat transfer fluid to provide freeze protection during colder months. The glycol water mixture is pumped through the FPC array, where it absorbs the incoming solar energy. The hot glycol water mixture then passes through the solar heating coils inside the storage tank where it exchanges heat with the tank water.

The natural gas burner is used to raise the tank temperature whenever the solar energy is insufficient to heat the tank to the required temperature of 60±0.5 °C. The hot water draw-off system consists of four solenoid valves that run parallel to each other, each with a different flow restrictor. The array of valves can be actuated in different combinations to achieve 15 distinct flowrates ranging from 0.94 to 16 liters per minute.

This arrangement provides the capability to simulate actual residential hot water draws. The opening and closing operation of the valves is controlled by a program written in LabVIEW software.

3.3.2. Instrumentation

The STWHS is equipped with a HOBO U30 station for monitoring and data logging sensors at a specific time interval. The station is configured with 14 data channels via a plug-in modular connector. The following system parameters are data logged: global solar radiation, collector outlet temperature, temperatures of glycol water mixture at the inlet and outlet of the solar coil, water temperatures at the top and bottom of the storage tank, cold water (building) inlet temperature, delivered hot water exit temperature, volumetric flow rate of glycol water mixture, and volumetric flow rate of natural gas.

The operation of the solar glycol loop is controlled by a Schüco IM TH3001 DeltaSol solar controller. The controller has a semiconductor relay which controls the operation of the solar pump based on the temperature difference between the solar fluid exiting the collector and water inside the storage tank. Three Pt1000 temperature sensors are connected to the solar controller to measure collector temperature, temperature of water at the top of the storage tank, and temperature of water at the bottom of the storage tank. A summary of all instruments data logged is provided in Table 3.1.

The circulating water glycol loop has a flow sensor that emits one pulse per gallon flow of glycol. Each pulse is sent to and recorded using the HOBO unit. Similarly, the AC-250 diaphragm gas meter is connected to the HOBO unit by a S-UCC-M006 pulse input adaptor. For each cubic foot of natural gas consumed, a pulse is sent to and recorded by the HOBO unit.

Table 3.1: Summary of measuring instruments.

Parameter measured	Sensor type	Sensor make/model	Measurement uncertainty
Glycol supply temperature	Thermistor	METRIMA SVM TDA	±0.15% (±0.02 °C)
Glycol return temperature	Thermistor	METRIMA SVM TDA	±0.15% (±0.02 °C)
Tank water inlet temperature	Thermistor	ONSET S-TMB-M002	±0.2 °C for 0 to 50 °C
Hot water exit temperature	Thermistor	ONSET S-TMB-M002	±0.2 °C for 0 to 50 °C
Solar radiation	Pyranometer	S-LIB-M003	±5% (±10 W m^{-2})
Volumetric flow rate of glycol	-	METRIMA SVM F2	±0.35%
Natural gas flow rate	Diaphragm meter	AC-250	-

All sensors were sampled at a 10-second interval. Physical properties of fluid, such as density and specific heat capacity were calculated at the corresponding fluid temperature. Energy and system efficiency values were calculated using the instantaneous experimental data collected under the outdoor conditions. To smooth the short-term fluctuations of the collected data, a 25-minute rolling average of the measured values was used in the data analysis.

3.4. Performance Metrics

As noted above, system performance data were collected for three different modes of operation: solar energy mode, natural gas energy mode, and hybrid (solar and natural gas) mode. The following performance metrics were calculated: energy delivered to the water tank, solar fraction, collector system efficiency, gas burner efficiency, and hybrid system efficiency, as described below.

3.4.1. Solar Mode of Operation

In the solar mode of operation, water inside the storage tank is heated using solar energy only. The rate of useful energy delivered by the solar fluid to the storage tank is calculated as [26] (Eq. 3.1):

$$\dot{Q}_d = \dot{m} C_{p,g} (T_{fi} - T_{fo}) \tag{3.1}$$

The collector system efficiency is calculated as shown in Eq. 3.2 [26]. This efficiency includes not only the efficiency of the collector itself, but also heat losses between the collector and storage tank, and the effectiveness of the solar heat exchanger located inside the storage tank.

$$\eta_s = \frac{\dot{m} C_{p,g} \left(T_{fo} - T_{fi}\right)}{A_c G_t} \tag{3.2}$$

3.4.2. Natural Gas Mode of Operation

In this mode of operation, water inside the tank is heated using natural gas energy. As reported by Aldrich [54], the burner efficiency (given by Eq. 3.3) is defined as the ratio of energy gained by the storage tank to the total natural gas energy supplied.

$$\eta_{burner} = \frac{m C_{p,w} (T_{ini} - T_{fin})}{V_{gas} * HV} \tag{3.3}$$

In this study, efficiency values are presented for both the higher and lower heating values of natural gas.

3.4.3. Hybrid Mode of Operation

In the hybrid mode of operation, water inside the storage tank is heated using both solar and natural gas energy. Solar fraction is defined as the ratio of the amount of energy provided by solar collector to the total energy required for water heating. It is calculated as [30] (Eq. 3.4):

$$f = \frac{Q_{solar}}{Q_{solar} + Q_{auxiliary}} \quad (3.4)$$

The rate of energy provided by solar collector was calculated using Eq. 3.1. The total solar heating time then multiplied this energy rate to calculate the total amount of solar energy delivered. The amount of auxiliary energy provided by gas heater was calculated by subtracting the energy delivered by solar collector from the total energy required for water heating.

3.4.4. Uncertainty Analysis

Experimental errors are unwanted but an inherent problem in an experimental data collection process. Experimental uncertainty due to calibration error, data recording error, and unsuitable instrument error might lead to misleading results. To reduce the effect of such experimental errors, each experiment was repeated four times. Uncertainty of all indirectly calculated values is reported following NIST guidelines [55], as discussed below.

In many cases, the desired result of a physical experiment is not directly measured but is derived using one or more directly measured variables. For example, the efficiency of the collector heating system, as shown in Equation 3.2, is not directly measured but is derived using directly measured values of mass flow rate, glycol inlet and exit temperature, and solar radiation. If a physical quantity Y is a function of n variables, X_1, X_2,…, X_n that are measured separately, the value of indirectly measured quantity Y can be calculated as [55] (Eq. 3.5):

$$Y = f(X_1, X_2, \ldots X_n) \quad (3.5)$$

Assuming the measured variables (X_1, X_2…, X_n) as uncorrelated and random, the combined uncertainty of the derived quantity Y can be calculated as [55] (Eq. 3.6):

$$U_Y = \sqrt{\sum_{i=0}^{n} \left(\frac{\partial y}{\partial x_i}\right)^2 {U_{X_i}}^2} \tag{3.6}$$

where $\left(\frac{\partial y}{\partial x_i}\right)$ represents the partial derivative of the function $f(X_1, X_2, \ldots X_n)$ with respect to the variable X_i and U_{X_i} represents the standard deviation of the measured variable X_i. Using this uncertainty propagation method, the uncertainty of derived variables, efficiency of collector, and gas-heater efficiency are calculated using built in capabilities of Engineering Equation Solver software [56] and reported in the following sections.

3.5. Results and Discussions

3.5.1. Solar Only Heating Mode

The efficiency of the solar collector heating system was measured at three initial tank temperatures of 20, 30, and 51.5 °C. The final temperature in all cases was 60 °C. These three cases are intended to simulate system performance for a full tank discharge and reheat (ΔT = 40 °C), recovery from a larger draw (ΔT = 30 °C), and recovery from a small draw or standby losses (ΔT = 8.5 °C). A summary of the results of the solar tests is shown in Table 3.2. Using the uncertainty propagation discussed above, the maximum uncertainty in the calculated efficiency was ±0.09%.

Table 3.2: Summary of solar tests

Initial Tank Temperature (±0.2 °C)	Range of Incident Solar Flux (±10 W m^{-2})	Number of Experiments Run	Range of Time to Heat Tank (hrs.)	Range of Overall Efficiency (%)
20.0	780 to 860	4	5.07 to 6.45	41.8 to 43.2
30.0	916 to 935	4	3.72 to 4.53	38.9 to 40.5
51.5	862 to 926	4	1.15 to 2.45	34.9 to 35.2

Figure 3.2 shows the solar radiation, mass flow rate of glycol, temperature difference between the glycol inlet and outlet temperature in the in-tank solar coil, tank water temperature, and collector heating system efficiency curve for a typical summer day (8/22/2017) with the storage tank initially at 20 °C. Data is presented with a 25-minute

rolling average applied. In this experimental run, it took approximately 6.32 hours to heat the tank water to the required temperature of 60 °C. The measured average solar radiation for the period of the experiment was 780 W m^{-2}. Depending on the intensity of solar radiation and the temperature of the water glycol fluid, the solar fluid mass flow rate varied between 42.5 and 63.7 g s^{-1}, with an average mass flow rate of 58.7 g s^{-1}. The average temperature difference between the glycol water mixture at the inlet and outlet of the tank solar coil was 10.15 °C. The average efficiency of the collector heating system (defined by Eq. 3.2) was found to be 41.83 %. The average efficiency is defined as the sum of all instantaneous (at every 10-second interval) efficiencies divided by the total number of data points during the solar heating time.

During the first few minutes of the test, the pump circulated the stagnant glycol water mixture, which had been preheated in the collector loop to a high temperature, to the water storage tank. This resulted in a larger than expected solar fluid temperature difference ($\mathrm{delta\ t},\ T_{fo} - T_{fi}$) in the first few minutes of the test and the unusual spike at the beginning of the efficiency curve shown in Figure 3.2. Once the stagnant glycol water mixture was fully circulated, the solar fluid temperature difference value became stable and representative of the instantaneous solar radiation.

According to Eq. 3.2, for a constant mass flow rate, instantaneous efficiency of a collector heating system depends on the solar fluid temperature difference and solar radiation. The effect of solar radiation on the collector system efficiency curve can be seen in Figure 3.2. It is seen that as the solar radiation value decreases, the collector system also decreases.

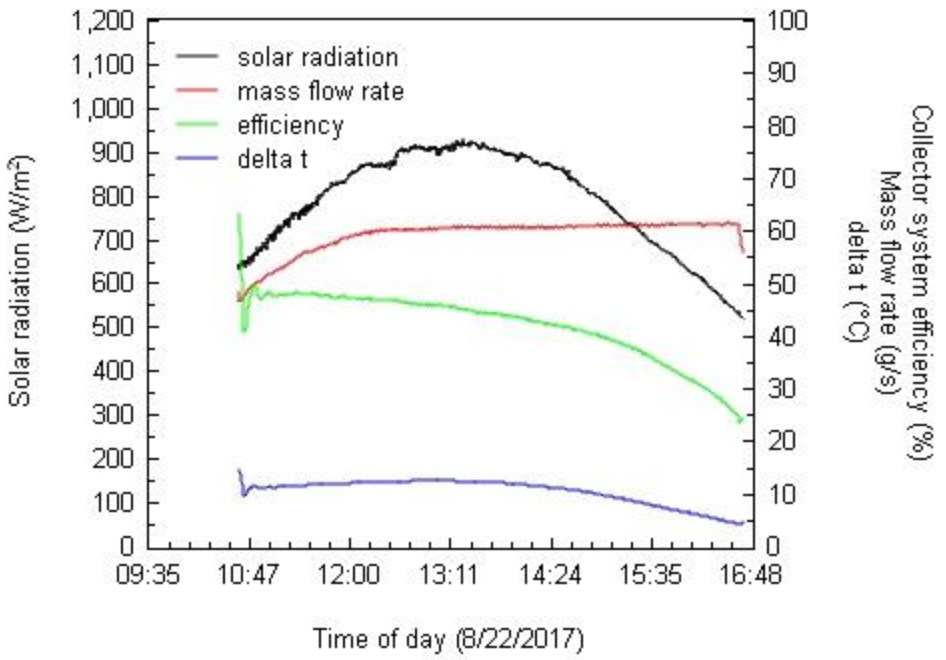

Figure 3.2: Collected sensor data and calculated efficiency values for a typical summer day (25-minute rolling average)

For steady-state operating conditions, the useful energy collected by an FPC under a near-normal incidence angle of solar radiation is calculated using Hottel-Whillier-Bliss equation as reported by Duffie and Beckman [26] (Eq. 3.7):

$$Q_u = F_R A_c [G_t(\tau\alpha) - U_L(T_i - T_a)] \tag{3.7}$$

As per Eq. 3.7, an FPC would collect the maximum possible energy if the temperature of fluid entering the collector (T_i) were always at a minimum possible temperature, or in other words, if the term $(T_i - T_a)$ in Eq. 3.7 was close to zero. However, the temperature of fluid entering the collector is not a design variable and cannot be controlled [57]. If we assume negligible piping heat losses and efficient heat exchange between the solar fluid and water, the collector fluid inlet temperature will be nearly equal to the storage tank temperature [57]. As the collector fluid inlet temperature increases, the collector heat loss value increases and, hence, less energy is collected. Moreover, in real life operating conditions, we cannot assume a constant heat transfer rate between solar fluid and water will occur. With an increase in tank water temperature and an approximately constant collector outlet temperature, the LMTD between solar fluid and tank water decreases, reducing the rate of heat exchange

between solar fluid and tank water. As a result, the efficiency of the solar heat exchanger decreases. For these two reasons, the efficiency of solar collector heating decreases with an increase in tank water temperature. This efficiency reduction was experimentally observed.

Figure 3.3 shows the average daily efficiency of the solar collector heating system for all four tests at different initial tank water temperatures and a final tank temperature of 60 °C. Taking into consideration that the average collector efficiency does not change significantly with change in solar radiation for a solar radiation range of 800 to 1100 W m^{-2}, it is seen that the efficiency of the collector heating system decreased with increase in tank water temperature. The efficiency of the collector heating system in completely heating water to 60 °C was found to be 42.01±0.09%, 39.82±0.08%, and 35.05±0.07% at initial water temperatures of 20±0.2, 30±0.2, and 51.5±0.2 °C, respectively. The reduction in efficiency with increasing inlet water temperature was expected and agrees with the trends cited in literature. Similar efficiency trends in terms of collector fluid inlet temperature were reported by You and Hu [58] and Celuppi et al [59].

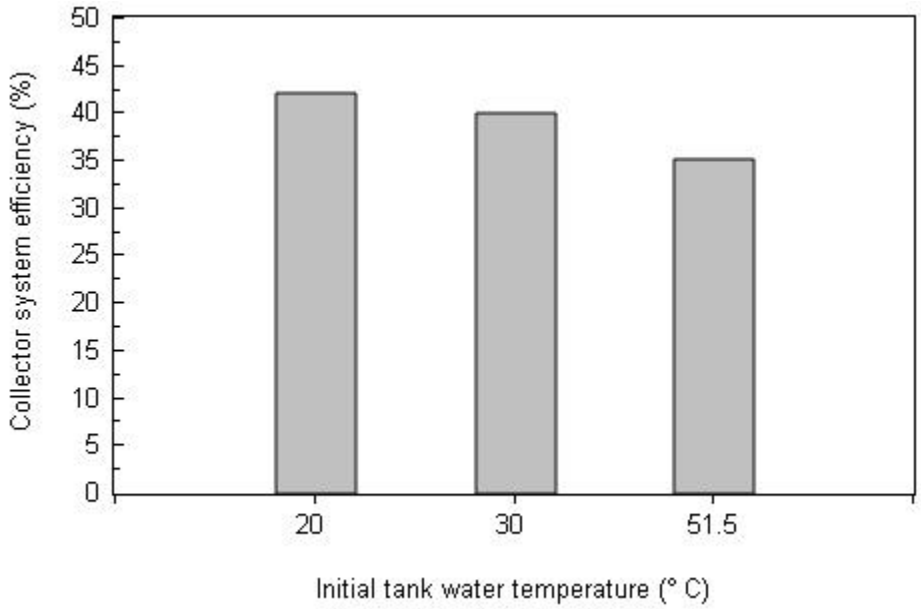

Figure 3.3: Collector system efficiency at different tank water temperatures

3.5.2. Natural Gas Burner Efficiency at Different Starting Temperatures

Using natural gas only, the tank water was heated to a final temperature of 60 ± 0.2 °C from three different inlet temperatures. Using Eq. 3.3, the efficiency of the gas burner was calculated and reported in terms of higher heating value (HHV) and lower heating value (LHV) of natural gas. The higher and lower heating values of natural gas used in the calculation were 52.225 and 47.141 MJ kg^{-1}, respectively [60]. The efficiency of the gas burner was found to be 69.20±0.14%, 66.41±0.13%, and 65.51±0.12% for HHV and 76.15±0.15%, 73.59±0.14%, and 72.60±0.14% for LHV for starting water temperature of 20, 30, and 51.5 ±0.2 °C, respectively.

The rate of heat transfer between combustion gases and tank water in a typical gas-fired water heater is given by:

$$\dot{Q}_t = UA \times LMTD \tag{3.8}$$

where LMTD is the logarithmic average of the temperature difference between water and combustion gases. For constant values of U and A, the larger the LMTD, the larger is the heat transfer rate.

Figure 3.4 shows the relationship between the gas burner efficiency and starting tank water temperature. It is seen that the efficiency of the gas burner is highest at an initial temperature of 20 °C and, as expected, decreases with increasing initial tank water temperature. As the tank water temperature increases, the temperature difference between the cold side (tank water) inlet temperature and hot side (combustion gas) exit temperature decreases. As a result, the temperature driving force of the heat exchanger (LMTD) decreases, decreasing the rate of heat transfer between combustion gases and water, and, hence, reducing the gas burner efficiency.

This efficiency reduction trend was expected and agrees with the trends cited in literature. For the same range of tank water temperature, similar efficiency reduction trends were reported by Maguire [53] and Makaire and Ngendakumana [21]. Other studies [52,61] reported the similar behavior for condensing gas boilers in terms of

return water temperature, and have suggested reducing the return water temperature to below 54 °C to achieve more favorable performance.

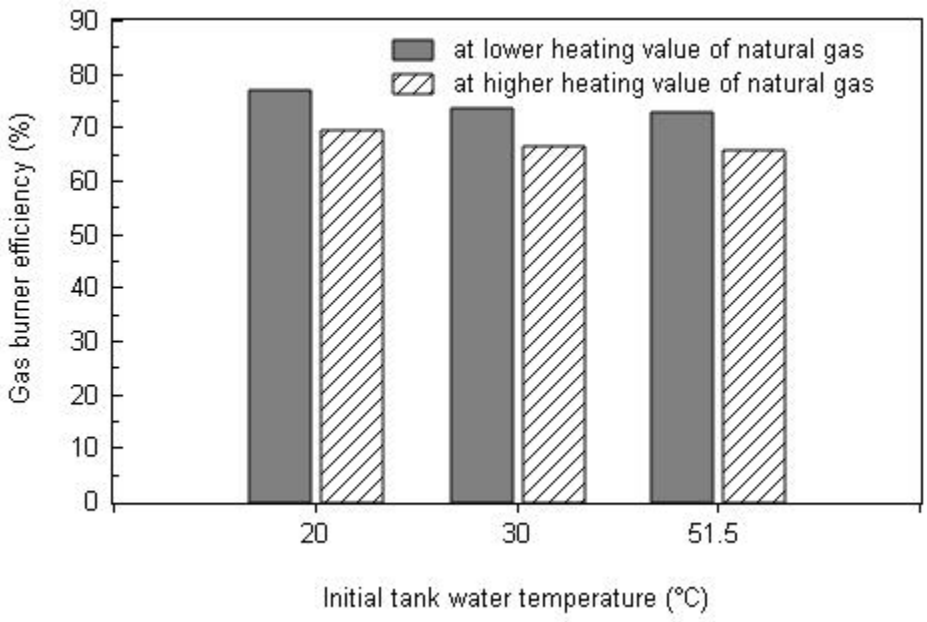

Figure 3.4: Natural gas burner efficiency for three different tank water temperatures

3.5.3. Combined Solar and Natural Gas

In the hybrid mode of heating, tank water initially at 20±0.2 °C was heated to 60±0.2 °C using both solar and natural gas energy, simultaneously. Four different solar radiation values representative of typical summer weather conditions in Corvallis, Oregon were used to analyze the performance of the hybrid solar/gas heating system. They consisted of heavily clouded sky (8/24/2017, 11:37 am to 12:34 pm), overcast sky (8/16/2017, 3:57 pm to 4:49 pm), clear sky (8/17/2017, 12:04 pm to 12:54 pm), and intermittent cloud covered sky (8/14/2017, 1:30 pm to 2:05 pm).

The solar radiation measurements during the tests were 489±10 W m^{-2} on the heavily clouded day, 616±10 W m^{-2} on the overcast day, 973±10 W m^{-2} on the clear sky day, and 787±10 W m^{-2} on the intermittent cloud covered day. Figure 3.5 shows the solar fraction and natural gas contribution at these solar radiation values. It is seen that with increasing solar radiation, a larger solar fraction is achieved, and, hence, less natural gas energy is required.

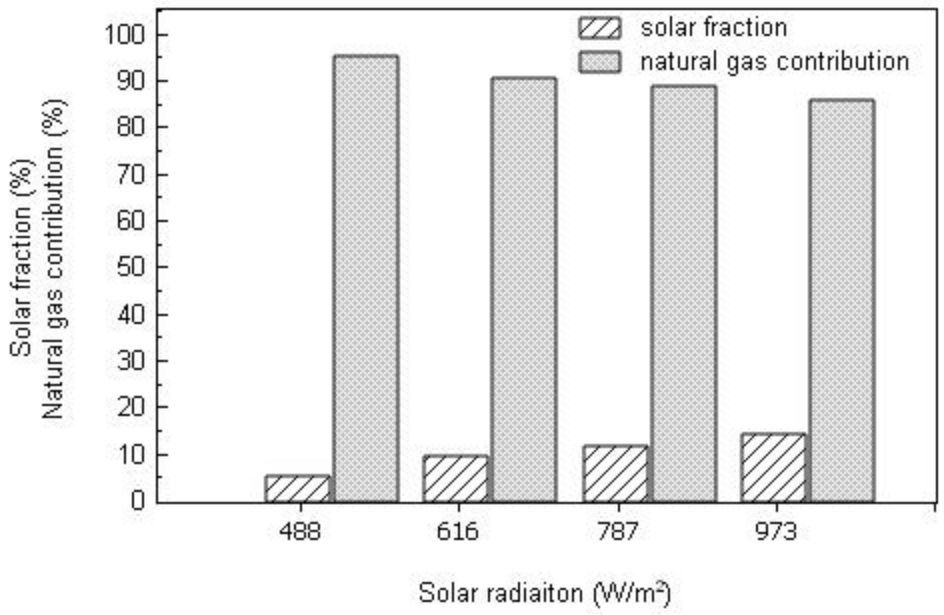

Figure 3.5: Solar fraction at different solar radiation values

However, as the solar fraction increases and the energy contributed by natural gas decreases, the efficiency of the gas burner also decreases. This occurs in the hybrid heating mode because the temperature of water in the tank increases due to the partial heating provided by the solar input. As a result, the temperature driving force, LMTD, for the gas burner becomes is reduced and the rate of heat exchange between the combustion gases and tank water decreases. The overall efficiency of the gas burner at different solar fraction values is shown in Figure 3.6. Based on the higher heating value of natural gas, the efficiency of the gas burner was found to be 69.08, 66.80, 66.17, and 65.18% at solar fractions of 4.93, 9.40, 11.39, and 14.27%, respectively.

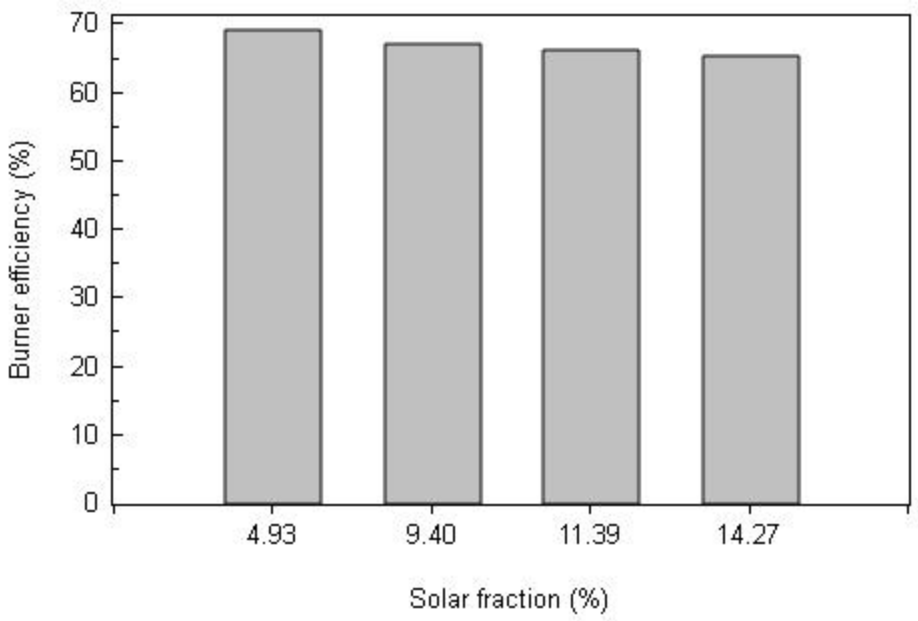

Figure 3.6: Gas burner efficiency at different solar fraction values

This set of experiments was conducted using the baseline control strategy where both natural gas and solar were used together to minimize tank heating time. In a real application, one may institute more sophisticated controls to use solar energy to heat tank to as high a temperature as possible, and then use gas to accomplish the final lift, increasing the solar fraction. However, even using this control strategy would result in a lower burner efficiency due to the decreased LMTD. This differs from a standard solar/electric heating hybrid, as noted above, where the auxiliary heating efficiency is relatively insensitive to tank water temperature.

3.6. Potential Improvements of the Hybrid System

3.6.1. Annual Gas Consumption at Different Solar Fraction and Inlet Water Temperature Values

According to ASHRAE handbook [62], the annual domestic 60 °C hot water demand of a typical US family is 86,140 liters. Using the burner efficiency values obtained through this experimental research, the volume of natural gas consumed by the solar/gas hybrid system to satisfy this hot water demand for varying initial tank temperatures and solar fractions was approximated. Three inlet tank water temperature (20, 30, and 51.5°C) scenarios were considered. The final water temperature was

assumed to be 60°C. For each inlet temperature, five different solar fractions (0, 25, 50, 75, and 100%) were assumed and the volume of natural gas consumed at corresponding solar fraction was calculated as (Eq. 3.9):

$$V_{gas} = (1 - f)\frac{mC_{p,w}(T_{ini} - T_{fin})}{\eta_{burner} * HV} \tag{3.9}$$

Figure 3.7 shows the relationship between solar fraction and volume of gas consumed by the solar/gas hybrid system for all three inlet water temperature scenarios. It is seen that the slope of the gas consumption curve decreases with an increase in inlet water temperature due to the decrease in gas burner efficiency with increasing inlet water temperature, as discussed above.

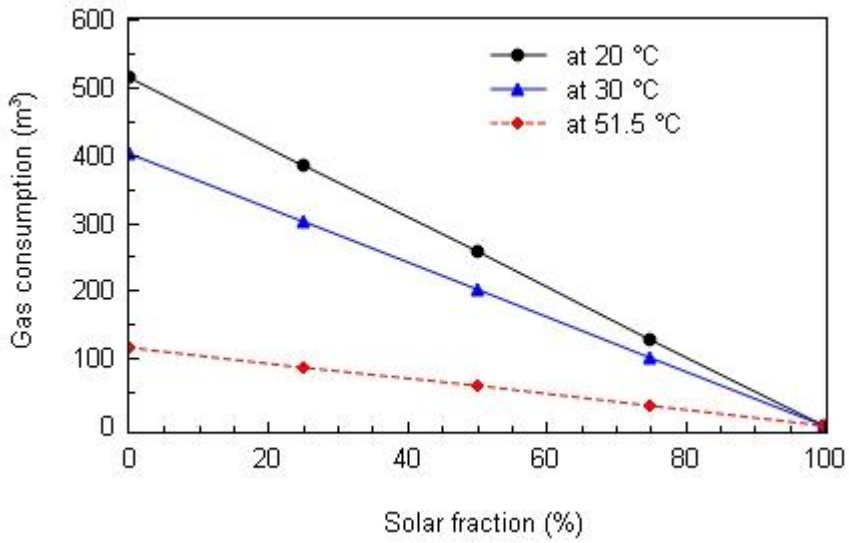

Figure 3.7: Approximate annual volume of natural gas consumed at three different initial water temperatures (all scenarios are for a final temperature of 60 °C).

The average volume of natural gas consumed by the hybrid system per degree of temperature rise is shown in Table 3.3. It is seen that for a higher initial tank water temperature, more natural gas is required per degree temperature rise. Hence, it is clear that lower inlet water temperature is desired to maximize gas burner efficiency and overall hybrid system efficiency.

Table 3.3: Natural gas consumption (m^3) per degree Celsius temperature rise

Solar fraction (%)	At 20 °C	At 30 °C	At 51.5 °C
	Burner efficiency of 69.23%	Burner efficiency of 66.43%	Burner efficiency of 65.50%
0	12.82	13.36	13.55
25	9.61	10.02	10.16
50	6.41	6.68	6.77
75	3.20	3.34	3.39
100	0.00	0.00	0.00

Based on the experimental study of the performance of the solar/gas hybrid system, there is clearly opportunity to explore new system configurations that maximize solar fraction while also maximizing efficiency of the gas auxiliary unit.

Under the current operational configuration of the hybrid system, the solar fraction can be maximized by using solar energy to heat the storage tank water to the required temperature, and when the solar input is not sufficient, the auxiliary gas burner would be turned on to top up the tank water temperature. However, as observed experimentally, the efficiency of the gas burner decreases at a higher starting water temperature. To avoid this inefficiency, it is suggested that instead of heating tank water that is pre-heated by solar input, the incoming cold water should be heated using an auxiliary gas burner and then mixed with heated water from solar storage tank on demand. This can be achieved by using a tankless gas-fired water heater and a thermostatic mixing valve as shown in Figure 3.8.

A storage gas water heater can be used as an alternative to an instantaneous burner. However, tankless water heaters have higher combustion efficiencies and eliminate standby losses that are common to storage water heaters [63].

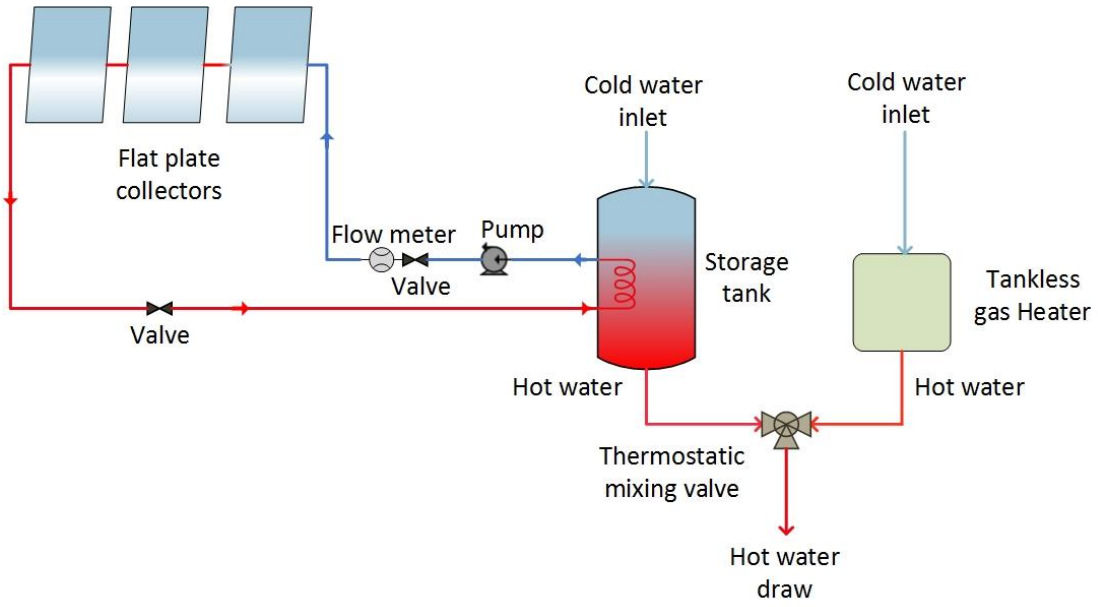

Figure 3.8: Proposed operation configuration

The operation of the thermostatic mixing valve can be controlled by using temperature sensors. A thermal-sensitive mechanism within the thermostatic mixing valve body automatically proportions the amount of hot water coming out of the solar heater and gas burner. The valve can be programmed such that when the temperature of the water exiting the solar tank falls below a minimum required temperature, the gas burner turns on to produce the required temperature blend. As observed experimentally, solar energy is usually enough to completely heat the tank to the required temperature during summer months. In contrast to this, solar fraction is typically low (0 to 25%) during winter months. So, a major proportion of hot water demand during winter would be provided by the gas heater. To maximize the use of the solar collector during the winter months, the minimum required temperature of water exiting the solar storage tank at the thermostatic mixing valve can be lowered.

The volume of natural gas consumed by the solar/gas hybrid system under the current and proposed configurations to satisfy annual hot water demand for a typical US family was calculated using Equation 3.9 and shown in Figure 3.9. Two different gas burner types, a tankless, instantaneous gas burner and the existing storage type gas burner, were considered as two alternative proposed configurations. The tank inlet water temperature and the tank exit water temperature were assumed to be 20 and 60 °C,

respectively. Five different solar fractions (0, 25, 50, 75, and 100%) were assumed. It is seen that less natural gas is consumed under the proposed configuration for both the instantaneous and existing storage burner compared to the current configuration, particularly in low and midrange (0 to 25%) solar fractions, which is typical of winter or spring season operation. Under the proposed configurations, the gas burner is always heating incoming cold water, thus operating at maximum possible efficiency. So, unlike in the current configuration where efficiency of gas burner decreases with increase in solar fraction, the efficiency of burner under proposed configuration remains constant regardless of changes in solar fraction. Natural gas savings offered by the proposed configuration with an instantaneous gas burner are higher than with existing gas burner because of its higher thermal efficiency [64].

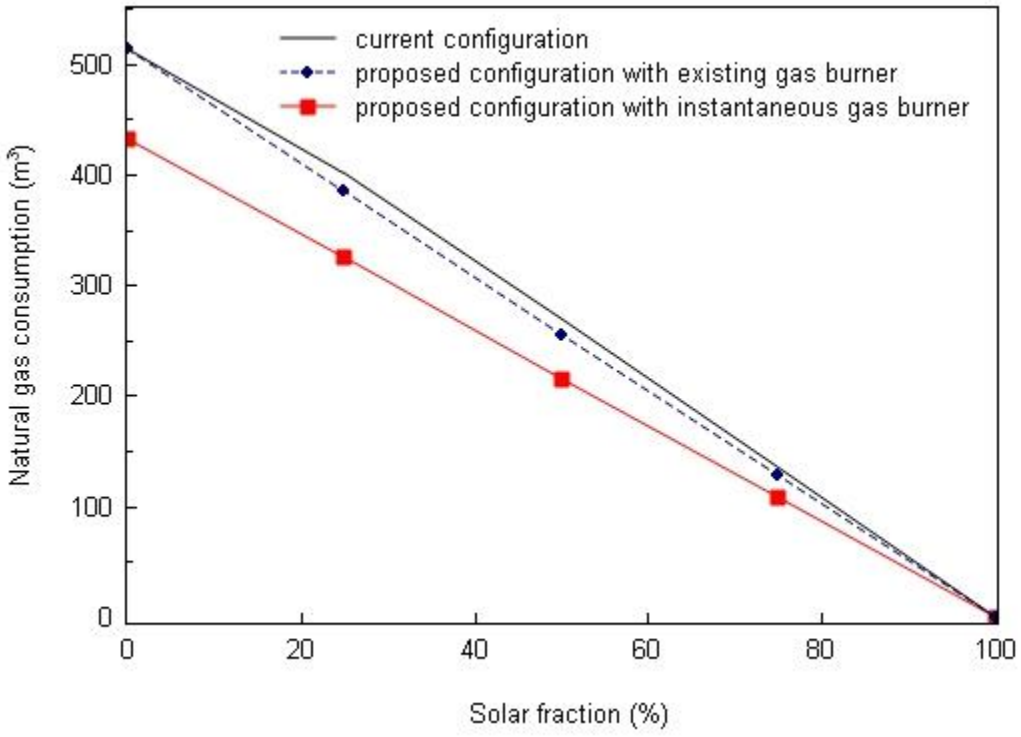

Figure 3.9: Approximate annual volume of natural gas consumed by the hybrid system under current and proposed configuration

The maximum difference in annual gas consumption between current configuration and proposed configuration with instantaneous gas burner in Figure 3.9 was obtained at solar fraction of 0% and found to be 80 m^3. This is approximately equivalent to 3240 MJ (30.68 therms) of energy in terms of HHV of natural gas. Similarly, the maximum

difference in annual gas consumption between current configuration and proposed configuration with existing burner was obtained at solar fraction of 25% and found to be 16 m^3 which is equivalent to 665 MJ (6.3 therms) of energy in terms of HHV of natural gas.

The initial cost of an instantaneous gas-fired water heater is usually higher than a traditional storage water heater. Instantaneous water heaters typically last longer and have lower energy costs, which could justify its higher initial cost [65]. Although the annual energy savings offered by the proposed configuration seems low, this value adds up to give a significant amount in the long run. Savings offered by the proposed configurations would be much higher if the system were used for industrial process heating where water heating load is much higher than domestic heating.

3.7. Conclusion

Performance of a solar/gas hybrid water heating system installed at Oregon State University in Corvallis, Oregon was monitored for a variety of typical weather conditions. Under different temperature lifts and solar insolation values, the hybrid system was operated at three different modes of heating: solar, gas, and combined solar/gas mode. Results showed that in the solar heating mode, the efficiency of the collector heating system was 41.97%, 39.82%, and 35.05% at starting water temperature of 20, 30, and 51.5 °C, respectively. For starting water temperatures of 20, 30, and 51.5 °C, the efficiency of gas burner was found to be 69.2%, 66.4%, and 65.5% at the HHV and 76.7%, 73.6%, and 72.6% at the LHV of natural gas, respectively. In the combined solar/gas heating mode, the efficiency of the gas burner decreased with increasing solar fraction. For solar fractions of 4.93%, 9.40%, 11.39%, and 14.27%, the efficiency of the gas burner in terms of the HHV of natural gas was found to be of 69.08%, 66.80%, 66.17%, and 65.18%, respectively.

Results from the experimental study showed that energy consumed by the gas heating system per degree temperature rise of tank water increases with increase in inlet water temperature. So, instead of heating water that is pre-heated by solar energy, it is recommended that the cold incoming water be heated separately and mixed with the solar tank water using a thermostatic mixer. Doing so will result in natural gas energy

savings when the solar/gas hybrid water heating system is operating at low and mid-range (15 to 50%) solar fraction, which is typical of spring and winter months. In addition to energy savings, the proposed configuration will also help to accurately quantify energy and cost savings offered by solar/gas hybrid system. This is because the efficiency of gas heater will remain constant (corresponding to the inlet water temperature) regardless of the solar input, making the prediction of cost and energy savings a very straight forward problem. This configuration is very useful in evaluating cost and energy savings during the feasibility assessment of solar/gas hybrid water heating systems.

3.8. Nomenclature

A_C	Collector aperture area (m^2)
C_P	Specific heat (J kg^{-1} K^{-1})
F_R	Collector heat removal factor
G_t	Solar irradiance (W m^{-2})
U_L	Collector overall heat transfer coefficient (W m^{-2} °C^{-1})
T	Temperature (°C)
$\dot{m}$	Mass flow rate (kg s^{-1})
$\dot{Q}$	Rate of useful energy collected (J s^{-1})
V	Volume (m^3)
HV	Heating value (kJ m^{-3})
Q	Energy (J)
F	Solar fraction (%)
A	Area of heat exchanger (m^2)
U	Heat exchanger overall heat transfer coefficient (W m^{-2}°C^{-1})
$LMTD$	Logarithmic mean temperature difference (°C)

Greek

η	Efficiency (%)
τ	Transmittance
α	Absorptance

Subscripts

U	Useful
I	Inlet
A	Ambient
G	Glycol
Co	Collector outlet

Ci	Collector inlet
Fi	Fluid inlet
Fo	Fluid outlet
C	Collected
D	Delivered
S	System
Burner	Natural gas burner
W	Water
Ini	Initial
Fin	Final
Gas	Natural gas
Solar	Solar heating system
auxiliary	Auxiliary heating system

CHAPTER FOUR: TECHNICAL AND ECONOMIC FEASIBILITY ASSESSMENT OF SOLAR THERMAL ENERGY SYSTEMS FOR SMALL AND MEDIUM SCALE MANUFACTURING ENTERPRISES

By

Saroj Karki, Karl R. Haapala, and Brian M. Fronk

To be submitted to the ISES *Solar Energy*

https://www.journals.elsevier.com/solar-energy

Chapter 4. Technical and Economic Feasibility Assessment of Solar Thermal Energy Systems for Small and Medium Manufacturing Enterprises

4.1. Abstract

Manufacturing industries require process heat for a wide variety of industrial operations, such as drying, cooking, washing, sterilizing, and pasteurization. Studies of industrial heating energy consumption have shown that more than 50% of the industrial heating demand is in the range of low (< 60 °C), medium (60 to 150 °C), and medium-high (< 250 °C) temperatures. A significant part of this low temperature thermal energy can be generated by commercially available solar flat-plate collectors, which would reduce the use of fossil fuels, energy cost volatility, and carbon emissions. However, manufacturing industries have not been able to take advantage of solar thermal energy systems for two main reasons: First, there is not enough information about when and what kind of systems can be economically applied; and second, manufacturing industries often do not have appropriate personnel or analysis tools to make decisions about installation of solar thermal systems. The goal of this research is to assist small- and medium-sized companies in conducting feasibility analysis for the application of solar flat-plate collector energy systems in their businesses by providing a design decision support tool. This research uses the $\bar{\phi}, f$-chart method and modified $\bar{\phi}, f$-chart design methods to predict the amount of energy collected by the solar thermal systems. To assess the economic feasibility of solar flat-plate collector energy systems, a simplified cost model is proposed. To demonstrate the methodology, an example decision support software application is presented, along with several what-if scenarios. A sensitivity analysis of savings-to-investment ratio (SIR) was performed by changing selected input parameters by ±30% from the base case. It was found that the SIR ratio was most sensitive to natural gas fuel cost followed by collector area dependent cost, discount rate, cost of any pre-heating system, and cost of the auxiliary gas heater.

4.2. Introduction

In the US, process heating operations, such as drying, cooking, washing, sterilizing, and pasteurization, are responsible for more energy demand than any other in the manufacturing sector, accounting for roughly 70% (7,204 TBtu in 2010) of the manufacturing sector process energy end use [66]. Several studies [10–13] of industrial heating energy consumption have shown that more than 50% of the industrial heating demand is in the range of low (<60 °C), medium (60 to150 °C), and medium-high (<250 °C) temperatures. The highest demand for low and medium temperature heat in US manufacturing industries is in the food, beverage, tobacco, paper, and textile industries [67]. A significant fraction of industrial heating energy, especially below 100 °C (212 °F), can be generated by commercially-available solar thermal technologies, which would reduce the use of fossil fuels, and the associated energy cost volatility and carbon emissions.

Application of solar thermal systems for domestic water heating is the most established technology with a proven record of performance worldwide [9]. Technically, compared to the domestic sector, the conditions for integration of solar thermal systems are more favorable in industrial sectors. Unlike in the domestic sector, where applications of solar thermal systems are limited to water heating, space heating, and swimming pool heating, industrial sectors have wider ranges of applications where solar thermal systems can be easily integrated. Another advantage of using solar thermal systems in industry is that industrial loads are often uniform throughout the year and coincide with solar hours (e.g., normal business hours of operation), which would result in better performance of solar energy collectors [12]. Despite the tremendous opportunity for energy cost reduction, the application of solar thermal systems for industrial process heating is rather unexploited compared to domestic heating applications. It has been estimated that solar energy incident on earth has the potential to fulfill the entire global thermal energy demand [68,69]. Yet, while an installed solar thermal capacity of 456 GWth was recorded worldwide at the end of 2016; industrial process heating accounted for only around 3% of the total installed capacity [8].

Three key barriers for large-scale deployment of solar thermal systems have been identified: technical, economic, and institutional barriers [69]. The most significant technical barrier is the inherently low solar thermal collector efficiency at higher collector inlet fluid temperatures—collector heat loss value increases with an increase in collector fluid inlet temperature, resulting in an efficiency reduction [26]. Other technical barriers include thermal losses, restriction in the heat carrying capacity of working fluids, and energy storage issues [70,71]. Economic barriers include a high initial cost of solar thermal systems [72], and a low cost of competing energy sources such as natural gas, resulting in long payback periods. Further, benefits of solar thermal systems, such as reduced greenhouse gas emissions and reduced reliance on fossil fuels, are difficult to quantify and are external to system users [72]. Therefore, the benefits are not internalized in the cost calculations [73]. Institutional barriers include lack of regulatory policies, such as carbon taxes [74] in the US. Enacting such laws can discourage the use of fossil fuels and encourage adoption of solar thermal systems. Other institutional barriers include limited understanding among key national and local institutions of basic technical system and economic (financial) factors [69].

Despite these barriers, studies in the US [75,76] have shown that solar thermal systems for industrial processes can be economically-competitive under certain conditions. However, manufacturing industries have not been able to take advantage of solar thermal systems for two main reasons. First, there is not enough information about when and what kind of systems can be economically applied. Second, manufacturing industries often do not have appropriate personnel or analysis tools to make decisions about the installation of solar thermal systems. To make a decision about installing a solar thermal system, it is necessary to assess the practicality of the system. Performance predictions at the site of interest and estimates of cost savings are the two most important factors considered in assessing the practicality of solar thermal systems. Unfortunately, feasibility studies of solar thermal systems require significant scientific and technical knowledge, and, hence, are costly. Small and medium-sized industrial enterprises, which are good candidates for installation of solar thermal systems, often lack the resources (e.g., worker time and skill) required for assessing solar thermal systems. Hence, they are not positioned to make investments in solar thermal systems.

The goal of this research is to develop a decision-support approach to assist small- and medium-sized companies in conducting feasibility analysis of application of solar thermal energy systems in their businesses. The paper is organized into five sections. The background section introduces the solar thermal systems technology and presents processes from several manufacturing sectors that are well-suited for the application of solar thermal energy systems. The research methodology section describes the methods used to predict the operational performance of solar thermal systems for applications in heating of low-temperature industrial process fluids. Next, to demonstrate the decision-support approach developed, an example software application is presented. Technical and economic analyses of a flat-plate solar thermal system are presented in the results section and include several what-if scenarios to aid discussion. Finally, key findings are provided in the conclusions section.

4.3. Background

Solar thermal technologies have been under development for many years to take advantage of the energy provided by the sun. This section describes a key element of these systems – solar collectors – as well as discussing the potential for solar thermal applications in manufacturing industry.

4.3.1. Solar Collectors

An industrial solar thermal energy system typically consists of a solar energy collector, a heat exchanger, an energy storage tank, and a control system [57]. The solar collector is a device that captures incident solar radiation and transfers the heat to a working fluid such as water of glycol/water mixture. Energy carried by the working fluid is then transferred to an energy storage tank using a heat exchanger. The performance of solar energy systems is measured in terms of solar fraction, which is defined as the fraction of total heat load that is contributed by solar collectors [30] to the total heat load. Solar fraction depends on many factors such as collector type and size, load, storage size, and available solar radiation.

As shown in Table 4.1, solar collectors can be classified as sun-tracking, collector type, absorber type, concentration ratio, and indicative temperature range collectors. Non-

tracking collectors are installed at a particular tilt angle and remain stationary irrespective to the position of the sun in the sky [77]. Concentration ratio is defined as the ratio of aperture area to the absorber area of the collector [27]. Both aperture area, the area of material (usually glazing) that collects the solar radiation, and absorber area, the area of material that actively converts solar irradiation into heat, vary depending on the design.

Table 4.1: Types of solar energy collectors [27]

Sun-tracking configuration	Collector type	Absorber type	Concentration ratio	Indicative temperature range (°C)
Non-tracking (Stationary)	Flat-plate collector (FPC)	Flat	1	30-80
	Evacuated tube collector (ETC)	Flat	1	50-200
	Compound parabolic collector (CPC)	Tubular	1-5	60-240
			5-15	60-300
Single-axis tracking	Linear Fresnel reflector (LFR)	Tubular	10-40	60-250
	Parabolic trough collector (PTC)	Tubular	15-45	60-300
	Cylindrical trough collector (CTC)	Tubular	10-50	60-300
Two-axis tracking	Parabolic dish reflector (PDR)	Point	100-1000	100-500
	Heliostat field collector (HFC)	Point	100-1500	150-2000

A flat-plate collector (FPC) is the most common type of solar collector appropriate for harvesting solar energy at temperatures ranging from 30 to 80 °C [30] and is the focus of this study. It is a low-cost option and can be used for a number of different applications that require low-temperature thermal energy, such as space heating and industrial process heating [57]. Information on other types of collectors is available from various sources [27,77].

4.3.2. Potential Applications of Solar Heat in Manufacturing

The industrial sector is the largest energy-consuming sector for heating, accounting for approximately 43% of global energy consumption in this manner [1]. Most industrial heating systems either partially or fully depend on carbon-based fuels to generate the required thermal energy [2]. Thus, renewable energy systems present an opportunity to reduce fuel consumption and carbon emissions.

Analysis of industrial energy consumption has shown that about 13% of the industrial heating applications require thermal energy at a temperature less than 100 °C [78] . Commercially-available solar flat-plate collectors can readily generate a significant portion of low-temperature industrial process heat [5]. Prior studies [10,11,15,79,80] have identified several manufacturing sectors and processes (Table 4.2) that are suitable candidates for application of solar flat-plate thermal energy systems. The following industrial sectors are identified as the most promising because of their low-temperature heat requirements: food and beverage, dairy, paper, textile, wood, and fabricated metal.

Table 4.2: Promising manufacturing sectors and process applications for solar flat-plate thermal energy systems [10,11,15,79,80]

Manufacturing Sector	Process	Temperature Range (°C)
Dairy	Cleaning	45-80
	Pressurization, Concentrates	60-80
	Pre-heating	60-90
Food and beverages	Smoking	20-85
	Washing	35-80
	Tempering	40-80
	Cleaning, Bleaching, Cooking	60-90
Textile	Washing	50-100
	Bleaching, Dyeing	60-90
Paper	De-inking	50-70
	Cooking, Drying	60-80
Fabricated metal	Chromate coating	20-75

	Pickling	20-100
	Electroplating, Phosphating	30-95
	Purging	40-70
Wood	Pickling	40-70
Machinery and equipment	Cleaning	40-90
Cross-industry	Washing	30-90
	Pre-heating feed and make-up water	30-100

Several studies have analyzed the feasibility of solar thermal systems for specific applications using detailed dynamic simulation programs. TRNSYS, the Transient System Simulation Tool [43], is one of the most commonly used software packages to simulate the behavior of solar thermal systems [81]. Benz et al. [24] performed TRNSYS simulations to design a solar thermal system for a bottle washing machine in a brewery and for a spray dryer in a dairy in Germany. Their study found that the efficiency of solar collectors for industrial process heating is comparable to the efficiency of solar collectors for domestic water heating. Kalogirou [10] analyzed the viability of a number of solar collector technologies with respect to life-cycle cost savings and energy yield for industrial process heating applications in Nicosia, Cyprus. Based on TRNSYS simulations, annual energy gains of 550 to 1100 kWh m^{-2} were predicted for an industrial application where 2000 kg hr^{-1} of hot water was needed at a temperature range of 60 to 240 °C. El Mkadmi & Wahed [23] performed TRNSYS simulations to study the performance of solar thermal systems in the dairy industry for three climatic conditions: Cyprus, France, and Morocco. They used optimization approach to design solar collectors and found the optimal design was able to meet 89. 76, and 94% of the total heating load for Cyprus, France, and Morocco, respectively.

In addition to TRNSYS, several other [82–84] simulation based decision support tools are available for dimensioning solar thermal energy systems. However, most of these simulation software tools are relatively expensive and specific for solar thermal design. More importantly, technical expertise is required to use simulation-based energy

system analysis tools. In addition, the possibility of waste heat recovery is another important aspect to be considered while designing and assessing the feasibility of solar thermal systems [25], which existing simulation-based decision support tool often do not consider.

Simplified decision-support tools, such as spreadsheet-based calculators, are lower-cost, require less computational speed, and can be used by an analyst with little technical experience. Such simplified decision support tools can quickly and accurately predict the results and, hence, can save the time and cost of a detailed pre-feasibility study. However, there is dearth of simplified decision support tools reported in the literature to help small and medium enterprises in assessing the feasibility of solar thermal systems for their individual applications.

4.4. Research Methods

In this study, the $\bar{\phi}, f$-chart method [57] and modified $\bar{\phi}, f$-chart [85] design method are implemented to estimate the amount of energy that would be collected by solar thermal energy systems for a given location. The $\bar{\phi}$, f-chart method is a simulation technique that uses empirical correlations derived from hundreds of simulations to predict the long-term performance of active closed-loop solar energy systems [57], shown schematically in Figure 4.1. The $\bar{\phi}$, f-chart is one of the most widely used methods to predict the annual performance of solar thermal systems [86]. This method requires the following inputs: collector properties, storage tank properties, heating load information, and climate data (monthly average ambient temperature and monthly average daily solar radiation information). This method calculates solar fraction (f) as a function of two dimensionless parameters: the ratio of collector losses to the heating load (X) and the ratio of absorbed radiation to the heating load ($\overline{\phi_{max}}\,Y$).

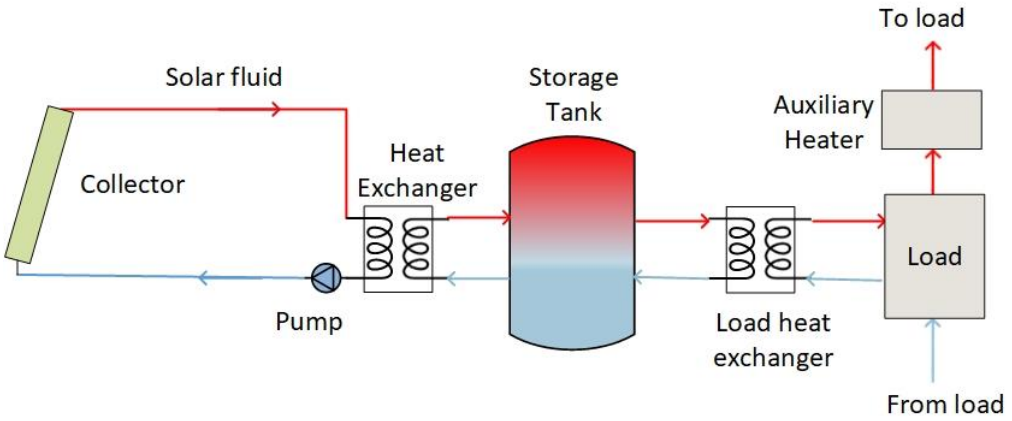

Figure 4.1: Schematic of a closed-loop solar thermal system

A schematic of an active closed-loop solar energy system defined by the $\bar{\phi}$, f-chart method is shown in Figure 4.1. In this schematic, energy absorbed by solar collectors is transferred to a solar fluid, which then passes through a heat exchanger to transfer the absorbed energy to the liquid inside a storage tank. The storage tank is assumed to be pressurized or filled with liquid of high boiling point so that minimal energy is lost through the pressure relief valve. A load heat exchanger is used to transfer energy from the storage tank to the load. An auxiliary heater is used in parallel with the solar energy system to provide additional heating whenever solar energy is insufficient to meet the heating demand. This method is particularly useful in simulating industrial process heating, space heating, and absorption refrigeration, where the load is relatively uniform [57].

As reported by Duffie and Beckman [26], for steady-state operating conditions, the rate of useful energy collected by a solar energy collector is calculated using the Hottel-Whillier-Bliss equation as (Eq. 4.1):

$$q_{useful} = F_R A_C [I_T(\tau\alpha) - U_L(T_i - T_a)]^+ \quad (4.1)$$

As shown in Eq. 4.1, the rate of useful energy collected by a solar energy collector is maximized when the temperature of the solar fluid entering the collector (T_i) is equal to a minimum possible temperature (T_{min}). However, T_i is not a design variable and cannot be controlled in practice [57] . Assuming negligible transfer losses and efficient heat exchange between the solar fluid and storage tank water, the temperature of solar

fluid entering the collector will be nearly equal to the water temperature in the storage tank [57] . As the solar fraction increases, the temperature of the storage tank, and thus the value of (T_i), increases, reducing the rate of useful energy collected. Therefore, nearly the maximum energy would be collected if the collected energy were used almost immediately (the storage tank temperature would remain equal to T_{min}), or if the storage capacity were very large, such that energy could be stored without raising the storage tank temperature much above T_{min} [57] .

The positive sign at the end of Eq. 4.1 indicates that only positive values are considered as useful energy. In other words, to collect any useful energy, the value of incident solar radiation must overcome the collector losses. The minimum solar radiation required to overcome collector losses when the fluid inlet temperature is equal to T_{min} is calculated as (Eq. 4.2) [57] :

$$I_{min} = \frac{F_R U_L (T_{min} - T_a)}{F_R(\tau\alpha)} \tag{4.2}$$

In terms of I_{min}, the rate of energy collected by a solar collector when T_i is equal to T_{min} is expressed as (Eq. 4.3):

$$q_{max} = F_R A_C (\tau\alpha)(I_T - I_{min}) \tag{4.2}$$

Integrating q_{max} over time, the maximum monthly average energy collected by a solar energy collector is calculated as (Eq. 4.4) [57] :

$$Q_{max} = A_C F_R (\overline{\tau\alpha}) \overline{H_t} N \overline{\phi_{max}} \tag{4.4}$$

The following steps (Eqs. 4.5-4.26) explain how $\overline{H_t}$ and $\overline{\phi_{max}}$ are calculated.

First, the declination value, δ, is calculated in degrees for any given day of the year (n) using Eq. 4.5. Declination (δ) is the angular position of the sun at solar noon with respect to the plane of the equator [26].

$$\delta = 23.45\, sin\left(360\,\frac{284+n}{365}\right) \tag{4.5}$$

The average value of n for each month can be obtained from the "Recommended Average Day for Each Month and Values of n by Months" table provided by Klein [87]. Sunset hour angle (ω_s) can be calculated using the equation (Eq. 4.6) devised by Cooper [88]:

$$\omega_s = \cos^{-1}(-\tan(\Phi)\tan(\delta)) \tag{4.6}$$

Knowledge of the amount of solar radiation available at a given location is fundamental to the design of solar energy systems and energy analysis models. To accurately predict the daily performance of a solar energy collector, it is first necessary to determine the amount of solar radiation available per day. As reported by Duffie and Beckman [26], the amount of daily extraterrestrial radiation incident on a horizontal surface, Ho, can be calculated as (Eq. 4.7):

$$H_o = \frac{24\times 3600 G_{sc}}{\pi}\left[1+0.033\,cos\left(\frac{360n}{365}\right)\right] \times\left[cos\Phi\, cos\delta\, sin\omega_s + \frac{2\pi\omega_s}{360}\, sin\Phi \sin\delta\right] \tag{4.7}$$

For a latitude range of 60°S to 60°N, using the monthly average values of n and δ, the monthly average daily extraterrestrial radiation ($\overline{H_o}$) incident on a horizontal surface can be estimated using Eq. 4.7 [26]. However, the amount of radiation that reaches Earth's surface is lower than H_o because a large part of the incident radiation is scattered, reflected back, and absorbed by the atmosphere [30]. The fraction of extraterrestrial radiation that reaches Earth's surface is defined as the clearness index (K_T) [26]. The monthly average clearness index ($\overline{K_T}$) for a location can be found using the equation (Eq. 4.8) proposed by Liu and Jordan [89] as:

$$\overline{K_T} = \frac{\overline{H}}{\overline{H_o}} \tag{4.8}$$

Normally, solar collectors are not installed horizontally but are installed at an angle to maximize the absorption of solar radiation and to reduce reflection losses [30]. Therefore, to accurately predict the amount of solar radiation that falls on a collector's surface, solar radiation incident on horizontal surfaces must be converted to the solar radiation values for tilted surfaces. Liu and Jordan [90] proposed an empirical method for the estimation of the monthly average daily total radiation incident on a tilted surface. According to their model, the ratio of average daily beam radiation on a tilted surface to that on a horizontal surface ($\overline{R_b}$) for each month can be calculated as (Eq. 4.9):

$$\overline{R_b} = \frac{\cos(\Phi - \beta)\, cos\delta cos\omega_s' + {}^{\pi}/_{180}\, \omega_s' \sin(\Phi - \beta)\, sin\delta}{cos\Phi cos\delta cos\omega_s + {}^{\pi}/_{180}\, \omega_s sin\Phi sin\delta} \tag{4.9}$$

where

$$\omega_s' = min\begin{pmatrix} \cos^{-1}(-tan\Phi\, tan\delta) \\ \cos^{-1}(-\tan(\Phi - \beta)\, tan\delta) \end{pmatrix} \tag{4.10}$$

Eq. 4.9 and Eq. 4.10 are only applicable for surfaces sloped toward the equator in the northern hemisphere, i.e., for surfaces with $\gamma = 0°$. For surfaces in the southern hemisphere sloped toward the equator (i.e., $\gamma = 180°$) refer to Duffie and Beckman [26].

The method presented by Liu and Jordan was extended by Klein [87], where the ratio of monthly average daily total solar radiation on an unshaded solar collector to the monthly average daily radiation, $\bar{R}$, is calculated as (Eq. 4.11):

$$\bar{R} = \left(1 - \frac{\overline{H_d}}{\overline{H}}\right)\overline{R_b} + \frac{\overline{H_d}}{\overline{H}}\left(\frac{1 + cos\beta}{2}\right) + \rho_g\left(\frac{1 - cos\beta}{2}\right) \tag{4.11}$$

where $\frac{\overline{H_d}}{\overline{H}}$ is the ratio of average daily diffuse radiation to monthly average daily radiation and is calculated using (Eqs. 4.12 to 4.13) [91]:

for $\omega_s \leq 81.4°$ and $0.3 \leq K_T \leq 0.8$,

$$\frac{\overline{H_d}}{\overline{H}} = 1.391 - 3.560\overline{K_T} + 4.189\,\overline{K_T^2} - 2.137\,\overline{K_T^3} \tag{4.12}$$

and for ω_s >81.4° and 0.3≤ K_T ≤0.8

$$\frac{\overline{H_d}}{\overline{H}} = 1.311 - 3.022\overline{K_T} + 3.427\,\overline{K_T^2} - 1.821\,\overline{K_T^3} \tag{4.13}$$

Utilizability (ϕ) is defined as the fraction of solar radiation incident on a collector's surface that is above a given threshold value (I_{min}) [87]. Maximum daily collector utilizability ($\overline{\phi_{max}}$) is defined as the sum over all hours and days of a month of the radiation falling on a tilted surface that is above I_{min} divided by the monthly average radiation [87]. The value of ($\overline{\phi_{max}}$) for a month depends on I_{min}, the distribution of hourly values of solar radiation in the month, and the location and orientation of the collector [57]. The procedure for calculating $\overline{\phi_{max}}$ developed by Klein [87] is explained below (Eqs. 4.14 to 4.26).

According to Collares-Pereira and Rabl [92], the ratio of total solar radiation for the noon hour to the total solar daily radiation for the month central day can be calculated as (Eqs. 4.14 to 4.16):

$$r_{t,n} = \frac{I}{H} = \frac{\pi}{24}(a^* + b^*)\frac{1 - \cos(\omega_s)}{\sin(\omega_s) - \frac{\pi\omega_s}{180}\cos(\omega_s)} \tag{4.14}$$

where, $$a^* = 0.409 + 0.5016\sin(\omega_s - 60) \tag{4.15}$$

and $$b^* = 0.6609 - 0.4767\sin(\omega_s - 60) \tag{4.16}$$

The ratio of diffuse solar radiation for noon to the total solar daily radiation for the month central day is calculated as (Eq. 4.17) [89]:

$$r_{d,n} = \frac{\pi}{24}\frac{1 - \cos(\omega_s)}{\sin(\omega_s) - \frac{\pi\omega_s}{180}\cos(\omega_s)} \tag{4.17}$$

As reported by Kalogirou [30], the ratio of beam radiation on the collector surface to that on a horizontal surface for the noon hour can be calculated as (Eq. 4.18):

$$R_{b,n} = \frac{(\sin(\Phi+\beta)\sin(\delta) + \cos(\Phi+\beta) * \cos(\delta) * \cos(h)}{\sin(\Phi) * \sin(\delta) + \cos(\Phi) * \cos(\delta) * \cos(h)} \quad (4.18)$$

According to Erbs et al. [91], the ratio of daily diffuse solar radiation to the daily radiation for the month central day is given as (Eq. 4.19):

For $\omega_s \leq 81.4°$,

$$\frac{H_d}{H} = \begin{cases} 1 - 0.272K_T + 2.4495K_T^2 - 11.95K_T^3 + 9.3879K_T^4 & for\ K_T < 0.715 \\ 0.143 & for\ K_T \geq 0.715 \end{cases} \quad (4.19)$$

For $\omega_s > 81.4°$,

$$\frac{H_d}{H} = \begin{cases} 1 + 0.283K_T - 2.5557K_T^2 + 0.8448K_T^3 & \text{for } K_T < 0.722 \\ 0.175 & \text{for } K_T \geq 0.722 \end{cases} \quad (4.20)$$

As reported by Duffie and Beckman [26], the ratio of noon hour total solar radiation on the collector to the noon hour total solar radiation on a horizontal surface, Rn, is calculated as (Eq. 4.21):

$$R_n = \left(\frac{I_t}{I}\right)_n = \left(1 - \frac{r_{d,n}H_d}{r_{t,n}H}\right)R_{b,n} + \left(\frac{r_{d,n}H_d}{r_{t,n}H}\right)\left(\frac{1+cos\beta}{2}\right) + \rho_g\left(\frac{1-cos\beta}{2}\right) \quad (4.21)$$

As reported by Kalogirou [30], the minimum monthly average critical radiation ratio is calculated as (Eq. 4.22):

$$\overline{X_{c,min}} = F_R U_L (T_{min} - \overline{T_a}) \quad (4.22)$$
$$\frac{3600}{\left(F_R(\tau\alpha)_n \times \left(\frac{\overline{\tau\alpha}}{(\tau\alpha)_n}\right) r_{t,n} \times R_n \overline{H} \times 1 \times 10^6\right)}$$

Finally, $\overline{\phi_{max}}$, as reported by Kalogirou [30] is calculated as (Eqs. 4.23 to 4.26):

$$\overline{\phi_{max}} = exp\left\{\left[a + b\left(\frac{R_n}{R}\right)\right]\left[\overline{X_{c,min}} + c\overline{X_{c,min}}^2\right]\right\} \tag{4.23}$$

where,

$$a = 2.943 - 9.271\overline{K_T} + 4.031\overline{K_T^2} \tag{4.24}$$

$$b = -4.345 + 8.853\overline{K_T} - 3.602\overline{K_T^2} \tag{4.25}$$

$$c = -0.170 - 0.306\overline{K_T} + 2.936\overline{K_T^2} \tag{4.26}$$

The value of $\overline{\phi_{max}}$ calculated using Eq. 4.23 would be for collectors for which $F_R(\overline{\tau\alpha})$ is equal to one and the fluid inlet temperature is equal to T_{min}. For a collector with zero heat loss coefficient ($U_L = 0$), the value of $\overline{\phi_{max}}$ is equal to one, and for collectors with non-zero heat loss coefficient ($U_L > 0$), the value of $\overline{\phi_{max}}$ will be less than one [57].

Next, Y is defined as the ratio of energy collected by a solar collector with zero heat loss coefficient to the monthly load, and is calculated as (Eq. 4.27) [57]:

$$Y = \frac{A_c F_R(\tau\alpha)_n \times \left(\frac{\overline{\tau\alpha}}{(\tau\alpha)_n}\right) \times r_{t,n} \times \bar{H}\bar{R}N}{L} \tag{4.27}$$

The product, $\overline{\phi_{max}}\,Y$, plotted on the ordinate of the $\bar{\phi}, f$-chart , gives the fraction of total load that would be supplied by a solar energy collector with specified values of $F_R(\tau\alpha)_n$ and $F_R U_L$ if the collector fluid inlet temperature were equal to T_{min}. However, in reality, collector fluid inlet temperature is greater than T_{min}. Assuming negligible transfer losses and an efficient heat exchange between the solar fluid and storage tank water, the collector fluid inlet temperature for a fixed storage capacity increases with increase in solar fraction [57].

The dimensionless parameter X, plotted on the abscissa of $\bar{\phi}, f$-chart, is defined as the ratio of collector energy loss at a reference temperature to the total heating load and is calculated as (Eq. 4.28) [57] :

$$X = \frac{A_c F_R U_L (T_{ref} - \overline{T_a})\Delta t}{L} \tag{4.28}$$

Based on hundreds of simulations, the value for the temperature difference between the reference temperature and ambient temperature $\left(T_{ref} - \overline{T_a}\right)$ was replaced by an empirical constant, 100 [57].

$$X = \frac{A_c F_R U_L (100)\Delta t}{L} \tag{4.29}$$

The value of X indicates the effect of collector fluid inlet temperature on the performance of a solar collector. The performance of a collector for which X is zero is unaffected by an increase in collector fluid inlet temperature. Assuming no storage tank energy losses, the solar fraction achieved by such a collector will always be equal to $\overline{\phi_{max}}$ Y [57]. In reality, because of unavoidable heat losses, collectors are sensitive to inlet water temperature and, thus, have a non-zero value of X.

The relationship of solar fraction (f) to the dimensionless variables $\overline{\phi_{max}}\,Y$ and X is referred to as the $\bar{\phi}, f$-chart and is analytically obtained as (Eq. 4.30) [57]:

$$f = \overline{\Phi_{max}}\,Y - 0.015(\exp(3.85f) - 1)(1 - \exp(-0.15X))R_s^{0.76} \tag{4.30}$$

The ratio, R_s, of standard storage heat capacity per unit of collector area (350 kJ m^{-2} °C^{-1}) to the actual storage capacity per unit of collector area is calculated as (Eq. 4.31) [57]:

$$R_s = \frac{350}{\frac{Mc_p}{A_c}} \tag{4.31}$$

The value of solar fraction calculated using the $\bar{\phi}, f$-chart method assumes there are no energy losses from the storage tank. However, in reality, there is some energy lost to the ambient from the storage tank, which is not accounted by the $\bar{\phi}, f$-chart method. Because of this, the solar fraction calculated using the $\bar{\phi}, f$-chart method is slightly

higher when compared to an actual system with storage tank losses. To account for storage tank losses, the following steps were proposed by Klein and Beckman [57].

The monthly total storage tank losses can be calculated as (Eq. 4.32) [57]:

$$Q_{st} = (UA)_t(\overline{T_s} - T_{env})\Delta t \tag{4.32}$$

As reported by Duffie and Beckman [26], the fraction of the total load supplied by the solar energy system, including storage tank losses, is calculated as (Eq. 4.33):

$$f_{TL} = \frac{L_s + Q_{st}}{L + Q_{st}} \tag{4.33}$$

Once the value of Q_{st} is computed, f_{TL} can be calculated using the $\bar{\phi}, f$-chart method for the new load of $L_s + Q_{st}$. Finally, the new solar fraction can also be represented in the form (Eq. 4.34) [26]:

$$f = f_{TL}\left(1 + \frac{Q_{st}}{L}\right) - \frac{Q_{st}}{L} \tag{4.34}$$

The value of Q_{st} cannot be directly calculated, but upper and lower value can be estimated. The lower bound of Q_{st} is calculated by assuming $\overline{T_s}$ remains at T_{min} and upper bound is calculated assuming $\overline{T_s}$ remains at the average collector fluid inlet temperature ($\overline{T_i}$). According to Klein and Beckman [57] the value of $\overline{T_i}$ can be calculated from $\bar{\phi}$-charts. Finally, the average daily utilizability is calculated as (Eq. 4.35):

$$\bar{\phi} = \frac{f_{TL}}{Y} \tag{4.35}$$

Once $\overline{T_i}$ is calculated, Klein and Beckman [57] recommended using the average of T_{min} and $\overline{T_i}$ in Eq. 4.31 to estimate the tank losses. Calculations from Eq. 4.32 to 4.35 are repeated until a satisfactory convergence of $\overline{T_s}$ is obtained.

The $\bar{\phi}, f$-charts were generated assuming there is no heat transfer resistance between the load and storage tank and, hence, the monthly solar fraction values calculated using

$\bar{\phi}, f$-charts are optimistic [57]. In practice, a load heat exchanger is employed between the storage tank and load. A load heat exchanger adds thermal resistance between the storage tank and load, which increases the storage tank temperature. As a result, there is an increase in the collector inlet fluid temperature and storage tank losses and, hence, a decrease in energy collected by the solar collectors. An average increase in tank temperature necessary to supply the required energy rate is calculated as (Eq. 4.36) [57]:

$$\Delta T = \frac{\frac{fL}{\Delta t}}{\varepsilon_L \, C_{min}} \tag{4.36}$$

The value of ΔT found using Eq. 4.36 is added to the T_{min} in Eq. 4.22 to calculate the value of $\overline{X_{c,min}}$.

The $\bar{\phi}, f$-chart method assumes that heating loads are relatively uniform every day. Therefore, this method will produce inaccurate results if the load distribution is highly irregular. In addition, this method does not account for energy dumping if the storage tank temperature exceeds 100 °C because this method assumes that the boiling temperature of storage tank is elevated. As a result, a slightly higher solar fraction is obtained during summer months compared to methods like TRNSYS simulation.

The $\bar{\phi}, f$-chart method in its original form is intended only for applications where the load can be characterized by a single temperature [57]. This method is not applicable for typical open-loop (no heat exchanger between the solar thermal system and load) water heating systems because water heating systems are characterized by two temperatures, supply water temperature and desired hot water temperature. To overcome this limitation, an improved method was proposed by Braun et al. [85], where a dimensionless correction factor Z was included in the $\bar{\phi}, f$-chart method.

The schematic of an open-loop water heating system defined by Braun et al.[85] is shown in Figure 4.2. In this system, a heat exchanger is used to transfer energy from the collector to a pre-heat tank. Water is drawn from the system if a desired temperature T_{set} is reached and is replaced with make-up water at temperature T_{mains}. If the solar

energy is not sufficient, an auxiliary water heater is operated to provide the additional energy. The mixing valve adjusts the temperature of delivered water to T_{set} if the temperature of water inside the pre-heat tank is greater than the desired temperature.

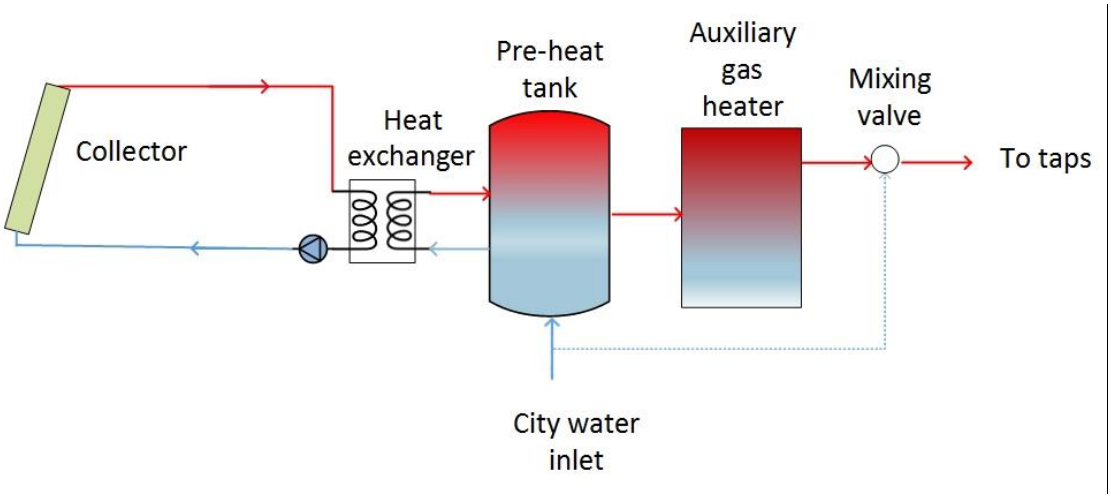

Figure 4.2: Schematic of an open-loop solar thermal system

The modified $\bar{\phi}, f$-chart method is applicable to both open-loop and closed-loop systems [85] . Under this method, useful energy collected by solar energy collectors is calculated as (Eq. 4.37) [85] :

$$Q_{useful} = Q_{max} - 0.015(\exp(3.85f) - 1) * (1 - \exp(-0.15X))\exp(-1.959Z)L \quad (4.37)$$

The dimensionless parameter Z in Eq. 4.37 is a measure of temperature rise required by the load and is calculated as (Eq. 4.38) [85] :

$$Z = \frac{L}{C_L(100\,°C)} \quad (4.38)$$

For an open-loop water heating system, C_L is calculated as (Eq. 4.39) [85] :

$$C_L = MC_P \quad (4.39)$$

For a closed-loop water heating system, C_L is calculated as (Eq. 4.40) [85] :

$$C_L = \epsilon C_{min} \tag{4.40}$$

The average storage tank temperature to consider storage tank losses is calculated as (Eq. 4.41) [85]:

$$\overline{T_s} = T'_{min} + g(\exp(4.702 * f) - 1)\exp(-4.002 * Z) \tag{4.41}$$

where

$$g = \frac{0.2136\,°C}{S_c * 350\frac{kJ}{m^2}°C} \tag{4.42}$$

To calculate the value of T'_{min}, an initial guess is made. Using the guessed value, an estimate of solar fraction is calculated as (Eq. 4.43) [85] :

$$f = \frac{MC_p(T'_{min} - T_{mains})}{L} \tag{4.43}$$

The values of Q_{useful} and $\overline{T_s}$ are then calculated using Eq. 4.36 and Eq. 4.40, respectively. A new estimate of solar fraction is then calculated as (Eq. 4.44) [85] :

$$f = \frac{Q_{useful} - (UA)_t(\overline{T_s} - T_{env})\Delta t}{L} \tag{4.44}$$

A new estimate of T'_{min} is then calculated as (Eq. 4.45) [85]:

$$T'_{min} = T_{mains} + \frac{fL}{MC_P} \tag{4.45}$$

For open-loop systems, solar fraction is calculated using Eq. 4.43 and for closed-loop systems, solar fraction is calculated using Eq. 4.44.

4.5. Results

To demonstrate the application of the modified $\bar{\phi}, f$-chart method for designing solar industrial process heating systems, we explore the representative case of a dairy. It is assumed that the dairy requires 10,000 L of hot water at 50 °C every day for floor

cleaning, which is a single-use purpose (open-loop system). Waste energy is available from other processes at the dairy. To recover this waste energy, a pre-heating system with a heat exchanger of 15 m^2 area is utilized. This heat recovery system will pre-heat the inlet water from 15 °C to 25 °C. A solar flat-plate collector water heating system, as shown in Figure 4.3, is then employed to heat the storage tank water from 25 °C to 50 °C. Design parameters for the system are given in Table 4.3. What-if analyses were conducted to evaluate the effect of geographic location, collector area, and collector tilt, as described next for this hypothetical design case. To facilitate analysis, a design decision support tool was developed in MS Excel. This tool is generally applicable for the evaluation of open- and closed-loop systems to evaluate various system design parameters and operational characteristics.

Table 4.3: Design parameters for solar flat-plate collector water heating system

Collector characteristics:	Collector area (A_c)	70 m^2
	$(F_R(\tau\alpha)_n)$	0.8
	Collector heat removal factor ($F_R U_L$)	4.17 W m^{-2} °C^{-1}
	Orientation	Slope = latitude
Storage tank characteristics:	S_c	350 kJ m^{-2} °C^{-1}
Heat loss conductance:	Pre-heat tank $(UA)_t$	10 W °C^{-1}
	Auxiliary tank $(UA)_a$	6.5 W °C^{-1}

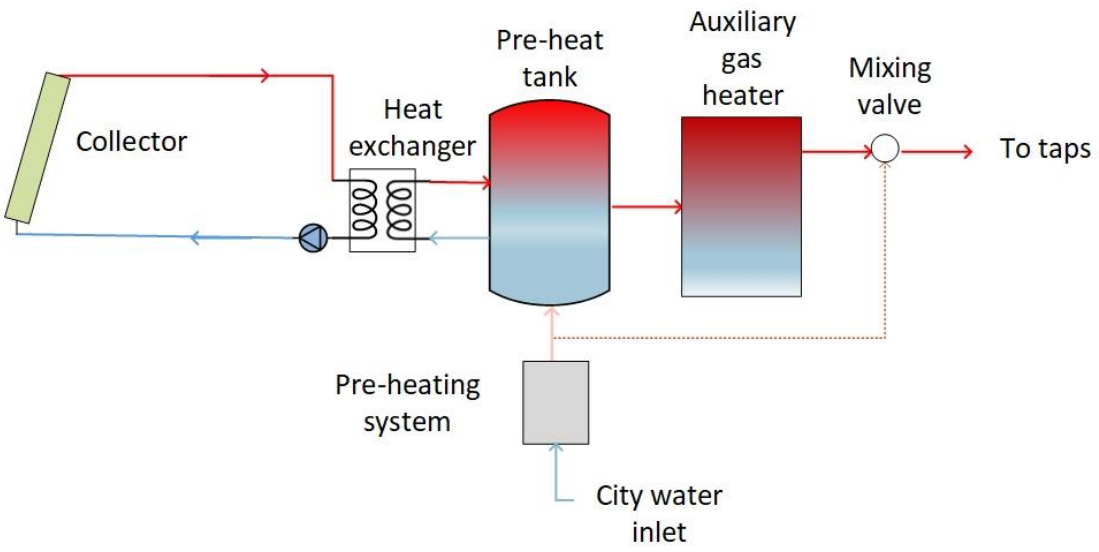

Figure 4.3: Schematic of solar-flat plate collector water heating system

4.5.1. Effect of Geographic Location on Solar Fraction

The decision support tool was utilized to calculate the solar fraction achieved by the solar water heating system described in Table 4.3. The analysis was performed for eleven US cities: Anchorage, AK (61.21°N), Chicago, IL (Central climate region, 41.87°N), Dallas, TX (South climate region, 32.77°N), Honolulu, HI (21.30°N), Madison, WI (East North Central climate region, 43.07°N), Miami, FL (Southeast climate region, 25.76°N), New York City, NY (Northeast climate region, 40.71°N), Omaha, NE (West north central climate region, 41.25°N), Phoenix, AZ (Southwest climate region, 33.44°N), Sacramento, CA (West climate region, 38.58°N), and Seattle, WA (Northwest climate region, 47.60°N). Each city (except for Honolulu and Anchorage) represents one of the nine climate regions in the US as defined by Karl and Koss [93]. Monthly average daily radiation and monthly average daily ambient temperature were obtained from NASA's surface meteorology and solar energy website [94].

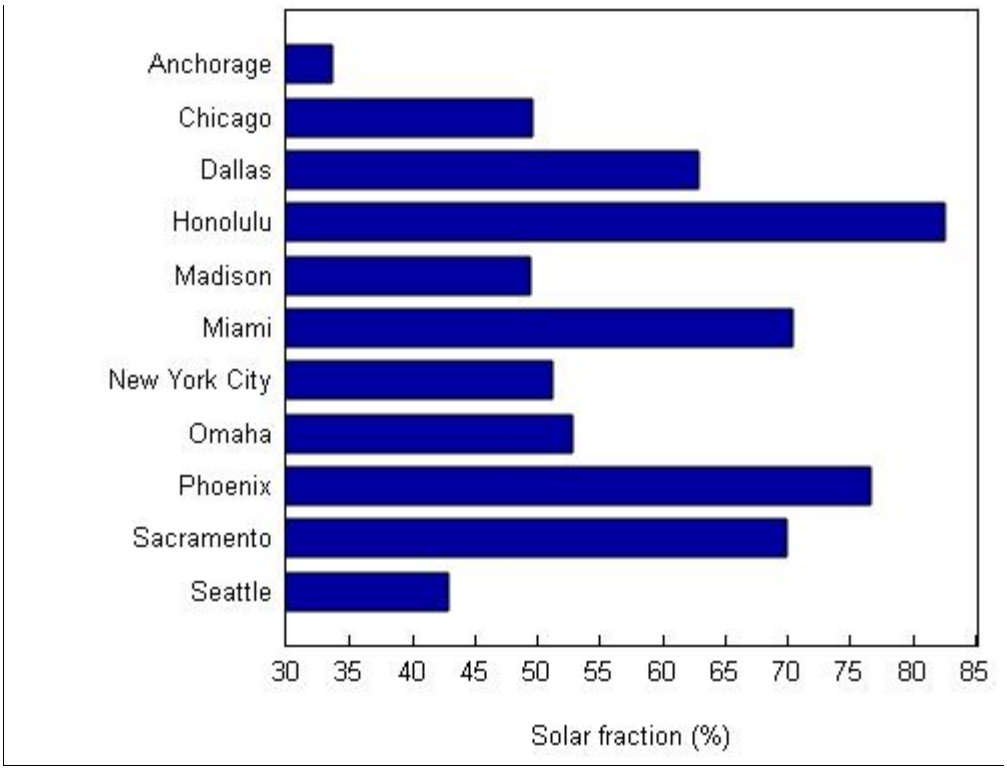

Figure 4.4: Annual average solar fraction at different locations

Figure 4.4 shows the annual average solar fraction achieved by the solar water heating system for all eleven US cities mentioned above. It is seen that maximum average annual solar fraction (82.6 %) was obtained for Honolulu. Here, the higher monthly average daily radiation and monthly average daily ambient temperature resulted in more energy collection and lower storage tank losses. Similarly, the minimum average annual solar fraction (33.6 %) was obtained for Anchorage due to the relatively lower monthly average daily radiation and monthly average daily ambient temperature. This analysis demonstrates how the developed tool can help industry practitioners identify whether solar flat-plate collectors would be adequate for energy collection with respect to their location and climate.

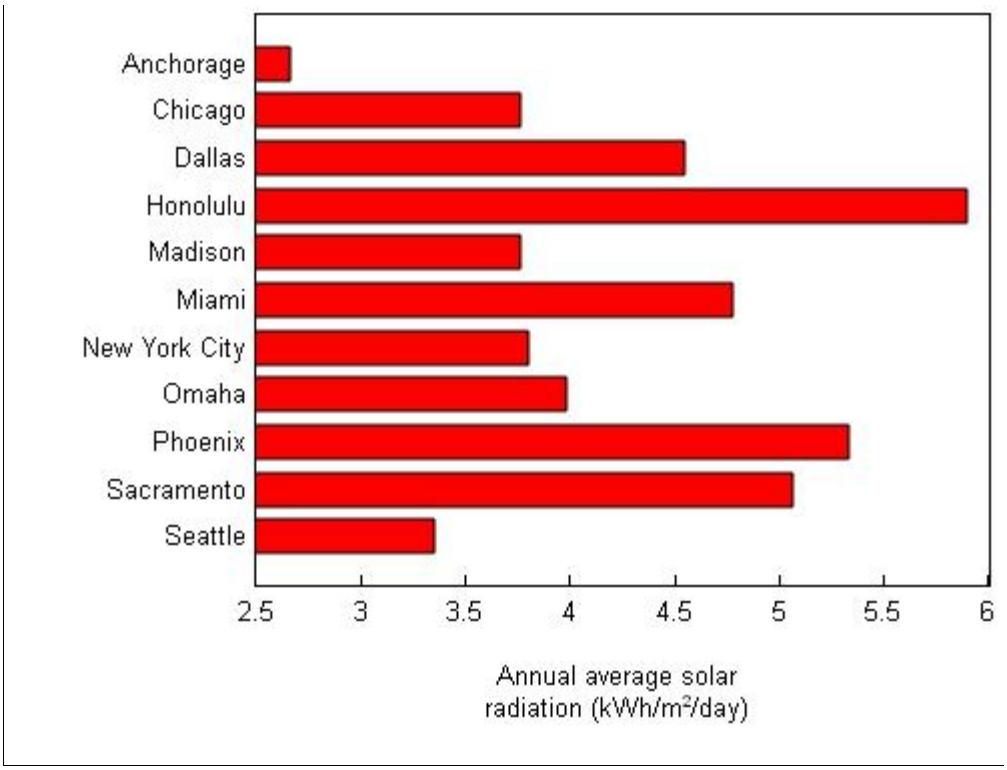

Figure 4.5: Annual average daily solar radiation at different locations

4.5.2. Effect of Collector Area on Solar Fraction

As described by Eq. 4.1, energy collected by solar collectors and, thus, solar fraction increases with increasing collector area. The decision support tool mentioned above was used to explore this effect. Figure 4.6 shows the general trend on the effect of increasing collector area on annual average solar fraction achieved. The analysis was performed using climate data for Honolulu, Omaha, and Anchorage—the locations with the maximum, median and minimum annual average solar fraction, respectively. It is seen that increase in collector area has largest effect on annual average solar fraction for Honolulu followed by Omaha and Anchorage. This is because of the larger annual average solar radiation available in Honolulu compared to Omaha and Anchorage. This analysis demonstrates that designing solar flat-plate collector energy systems with large collector area values for locations with lower annual average solar radiation might not be as beneficial (in terms of improved annual average solar fraction) as compared to locations with higher annual average solar radiation values.

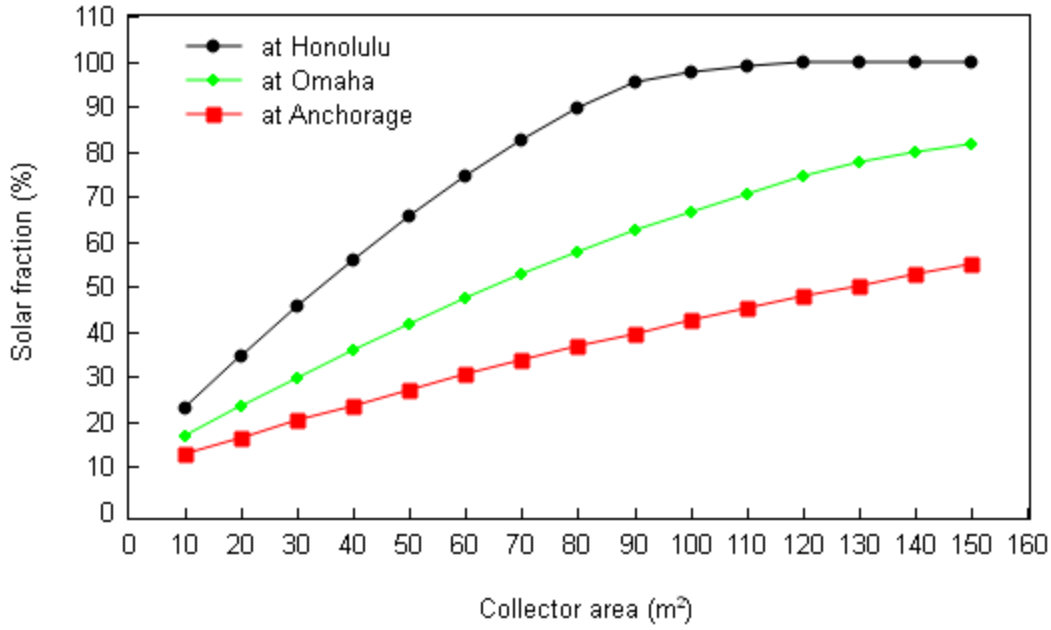

Figure 4.6: Annual average solar fraction at different collector area values

Figure 4.7 shows the monthly average solar fraction achieved by the system defined in Table 4.3 for collector areas of 30, 50, 70, and 90 m^2. Climate data for Honolulu was used to perform the analysis because of its larger annual average daily solar radiation values. As expected, it is seen that the monthly average solar fraction value increases with increase in collector area. However, since the maximum possible solar fraction is 100%, increasing collector area to 90 m^2 may indicate that it is oversized. The solar collector contributes to 100% of the heating between April and September, and is likely overheating the water, requiring cooling water to be used, for example. This analysis can help industry practitioners dimension the size (area) of solar flat-plate collector based on the desired solar fraction.

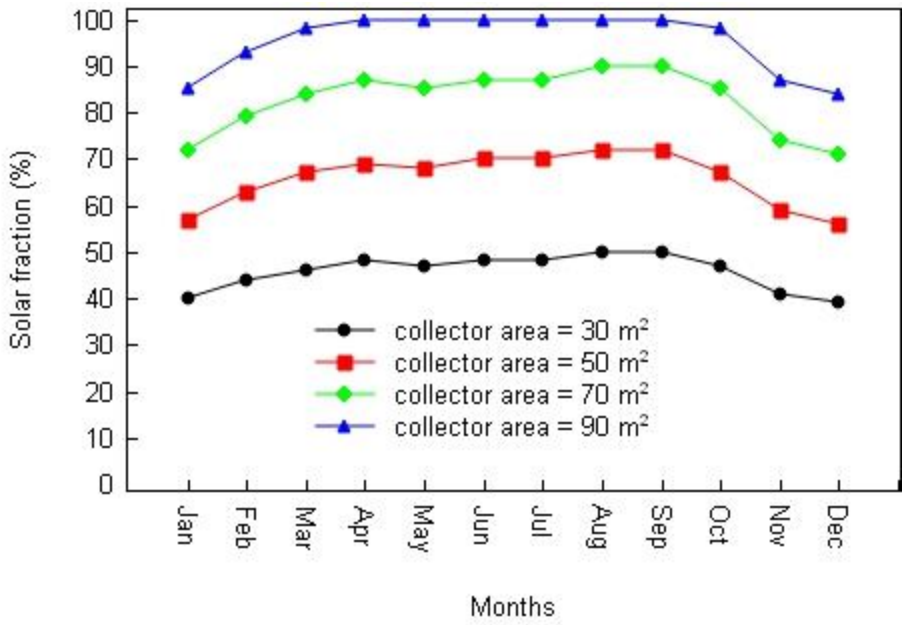

Figure 4.7: Monthly average solar fraction at different collector area values for Honolulu

4.5.3. Effect of Collector Tilt Angle on Solar Fraction

In the northern hemisphere, the optimum collector orientation is south facing, and the optimum collector tilt angle is higher (usually 15° more than the location's latitude) for winter months and is lower (usually 15° less than the location's latitude) for summer months [95]. The best way to achieve an optimal tilt is by using solar tracking systems but, tracking systems are expensive and not always applicable [96].

Figure 4.8 shows the solar fraction achieved by the above-mentioned system using climate data for Honolulu for three different collector tilt angles: 5° (~latitude-15°), 20° (~latitude), and 35° (~latitude+15°). As expected, it is seen that the lower tilt angle resulted in higher solar fraction in summer and higher tilt angles resulted in higher solar fraction in winter. Overall, a higher average annual solar fraction was achieved for tilt angle equal to latitude. This follows the general recommendation for a stationary flat-plate collector, where collector tilt angle equal to the local latitude is advised [97].

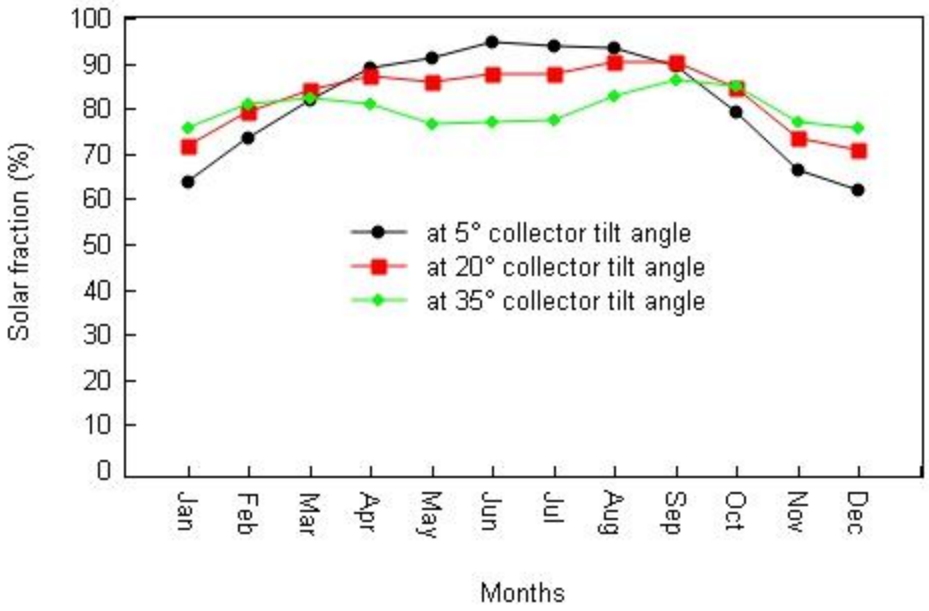

Figure 4.1: Monthly average solar fraction at different collector tilt angle values

4.5.4. Economic Analysis of Solar Flat-Plate Collector Energy Systems

A simplified cost estimation model to assess the economic feasibility of solar flat-plate collector systems is presented next. The total cost of the solar flat-plate collector water heating system shown in Figure 4.3 can be represented as the sum of the costs of three subsystems: the flat-plate collectors, auxiliary natural gas heating system, and pre-heating system (Eq. 4.46).

$$TC = C_{FPC} + C_{GH} + C_{HR} \tag{4.46}$$

The total cost of solar flat-plate collectors (C_{FPC}) can be represented as the sum of two different costs: the initial system cost and the cost of operation and maintenance (Eq. 4.47).

$$C_{FPC} = C_{SI} + C_{O\&M} \tag{4.47}$$

The initial cost of a solar flat-plate collector system (C_{SI}) depends on several factors, such as the costs of solar flat-plate collectors and the collector structure system, installation cost, cost of the solar controller, piping and insulation costs, cost of the solar pump, cost of the solar heat exchanger, and cost of the storage tank [26]. These

system costs can be divided into two main categories: collector area dependent costs (C_a) and collector area independent costs (C_f), as shown in Eq. 4.48 [26]:

$$C_{SI} = C_a\, A_C + C_f \tag{4.48}$$

The cost of an auxiliary gas heating system (C_{GH}) is represented as the sum of initial installation cost (C_{GI}) and the operating cost(C_{OP}) and is calculated as (Eq. 4.49) :

$$C_{GH} = C_{GI} + C_{OP} \tag{4.49}$$

The initial installation cost is calculated as (Eq. 4.50):

$$C_{GI} = S_{GH} \times C_H \tag{4.50}$$

The annual operating cost is calculated as (Eq. 4.51):

$$C_{OP} = \frac{E_R}{\eta_H} \times NG_R \times t_O \tag{4.51}$$

The pre-heating system is a heat exchanger that recovers waste heat to pre-heat the incoming city water. The cost of a pre-heating system is calculated as (Eq. 4.52):

$$C_{HR} = A_{HE} \times C_{HE} \tag{4.52}$$

The total cost of the solar flat-plate collector water heating system throughout its useful life is selected and calculated as a performance indicator for the economic analysis herein. To illustrate the general cost trends, some simplifying assumptions are made. It is assumed that all initial investment costs for the solar flat-plate collector water heating system are incurred at the beginning of the project. The average life expectancy of gas heater is typically lower compared to solar flat-plate collectors. However, since the gas heater is used in conjunction with solar collectors, it is assumed that the heater will be used less often and hence, have a prolonged life. The period of the economic analysis (useful life of the system) is taken as 25 years [98]. This analysis assumes a linearly increasing cost of solar collectors, which may not be realistic. The operation and

maintenance costs of solar flat-plate collectors are assumed to be constant throughout the useful life and equal to 2% [99] of the initial capital cost. The maintenance costs of the auxiliary gas heating system and heat recovery system is assumed to be negligible and is not considered in the cost analysis. Both replacement cost and salvage value of the solar flat-plate collector water heating system are ignored in this cost analysis.

The present worth (PW) of all costs calculated in Eq. 4.46 is calculated using Eq. 4.53:

$$PW = \sum_{i=1}^{25} \frac{1}{(1+d)^j} \tag{4.53}$$

Annual cost savings offered by solar flat-plate collector water heating system described in Table 4.3 is calculated as (Eq. 4.54):

$$C_S = \frac{(E_{with\ solar} - E_{without\ solar}) \times NG_R \times t_O}{\eta_H} \tag{4.54}$$

The annual cost savings are calculated based on the following assumptions: natural gas is used as the fuel for providing auxiliary water heating energy, and energy savings are calculated by comparing the system shown in Figure 4.3 with a natural gas heating system with a pre-heater.

Savings-to-investment (SIR) ratio is defined as the ratio of the present value of the total annual savings throughout the useful life to the present value of total life-cycle costs (Eq. 4.55):

$$SIR = \frac{PW\{C_{S-life}\}}{PW\{TC_{life}\}} \tag{4.55}$$

A SIR greater than one indicates that a solar flat-plate collector system is economically feasible. Cost parameter values used in the economic analysis are summarized in Table 4.4.

Table 4.4: Cost parameters for the economic analysis

Description	Symbol	Value	
Area-dependent cost ($/m^2)	C_a	*750	[100]
Area-independent cost ($)	C_f	5,000	[100]
Cost of natural gas heater ($/kW)	C_H	102.36	[101]
Efficiency of gas heater	η_H	0.8	[64]
Annual operating days	t_o	365	
Cost of heat exchanger ($/m^2)	C_{HE}	900	[102]
Discount rate (%)	D	5	[103]

* Collector area-dependent costs are reported in the range of $250 to $1100 /m^2 [104]. A higher value is used in this analysis as a conservative estimate.

4.5.4.1. Total Life-Cycle Cost for Different Collector Areas at Different Locations

The present worth of the total life-cycle cost of the solar flat-plate collector water heating system described in Table 4.3 was calculated for different collector area values and is reported in Figure 4.10. The cost calculations were performed using climate data for Honolulu, Omaha, and Anchorage—locations with maximum, median, and minimum annual average solar fractions, respectively, as discussed in Section 4.5.1.

Cost parameters summarized in Table 4.4 were used to calculate the total cost of the system. The price of natural gas (NG_R) was assumed as the average industrial natural gas price for each location over the past three years (2015-2017), as reported by the US EIA [67].

As defined in Eq. 4.48, the installation cost of solar flat-plate collectors increases linearly with increasing collector area. This cost is assumed to be the same for all three locations. Similarly, since a constant heat exchanger area is used, the cost of pre-heating system remains same for all collector area values and for all locations. The only cost values that vary with locations are the installation and operation costs of the auxiliary gas heating system (shown in Figure 4.9).

As discussed in Section 4.5.2, with an increase in collector area, a higher solar fraction is achieved, and less natural gas is required to satisfy the heating demand, resulting in

a smaller auxiliary heating system and lower associated cost. As discussed in Section 4.5.1, for a given collector area, the solar fraction achieved by the system is largest for Honolulu, followed by Omaha and Anchorage. Therefore, the system in Honolulu has a lower auxiliary energy cost, followed by Omaha and Anchorage. For the same reason, it is expected that the value of energy and cost savings achieved by the system will be largest for Honolulu, followed by Omaha and Anchorage for the same collector installation cost.

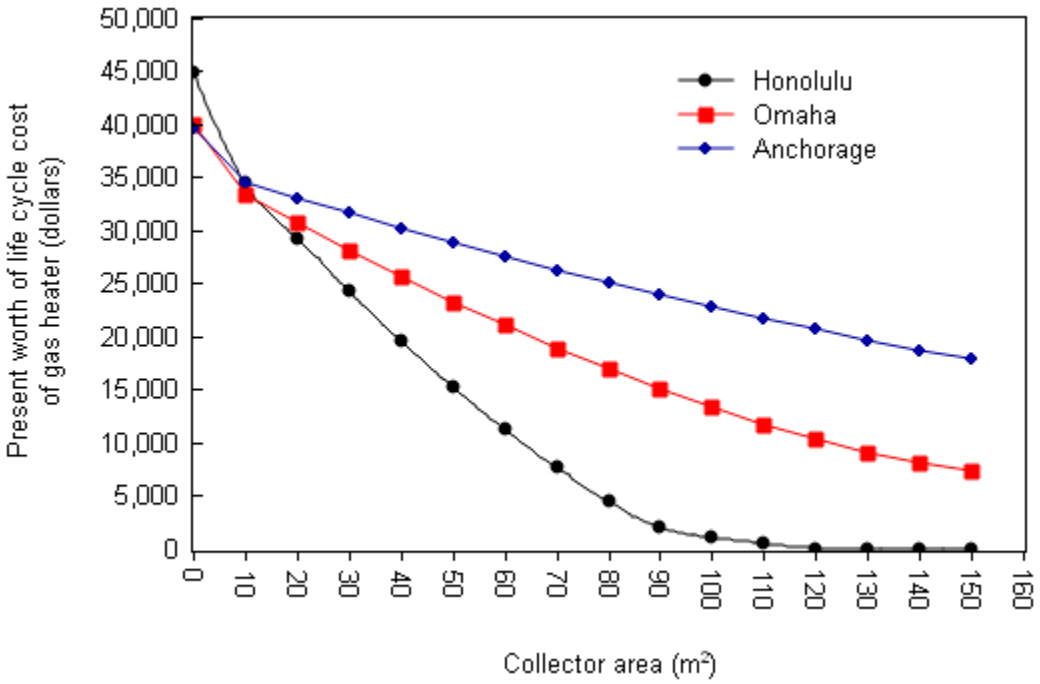

Figure 4.2: Effect of collector area on life-cycle cost of an auxiliary gas heating system for three selected locations

Initially, the life-cycle cost of a gas heating system (up to collector area of 10 m^2) is higher in Honolulu compared to Omaha and Anchorage. The higher initial cost is due to the higher natural gas price in Honolulu (0.057 $/kWh) compared to Omaha (0.021 $/kWh) and Anchorage (0.018 $/kWh).

The sum of present values of life-cycle costs of all three individual components (solar collectors, pre-heating system, and auxiliary gas heating system) is calculated for all three locations at different collector area values and is shown in Figure 4.10. Because natural gas is expensive in Honolulu and because a larger solar fraction can be achieved

at relatively low collector area in Honolulu, total life-cycle cost can be reduced by adding solar collector area (up to collector area of 80 m^2 in this case). However, as shown in Figure 4.6, the rate of increase in solar fraction achieved by the system per unit collector area increase decreases with increasing collector area beyond 80 m^2. Beyond this point, the auxiliary energy cost savings achieved upon further addition of solar collectors becomes smaller than the marginal collector installation cost, resulting in an increase in the total system cost. This results in a minimum total life-cycle cost for a collector area of 80 m^2 in Honolulu (corresponding solar fraction = 90%, corresponding SIR = 0.83).

However, a different trend is observed for Omaha and Anchorage. As discussed in Section 4.5.2, the rate of increase in solar fraction per unit collector area increase is smaller for Omaha and Anchorage compared to Honolulu. Additionally, the price of natural gas for both locations is lower compared to Honolulu. Due to the combination of these two factors, the cost of installing solar collectors becomes higher than the auxiliary energy cost savings achieved by the system. Hence, an increasing trend for total life-cycle cost is observed. The present value of total life-cycle cost (for Omaha and Anchorage) is smallest for collector area of zero m^2 (no solar thermal system, preheating system, and gas burner only). This indicates that for the price of natural gas used in this analysis, it is advantageous, in terms of total life cycle cost, not to install solar collectors.

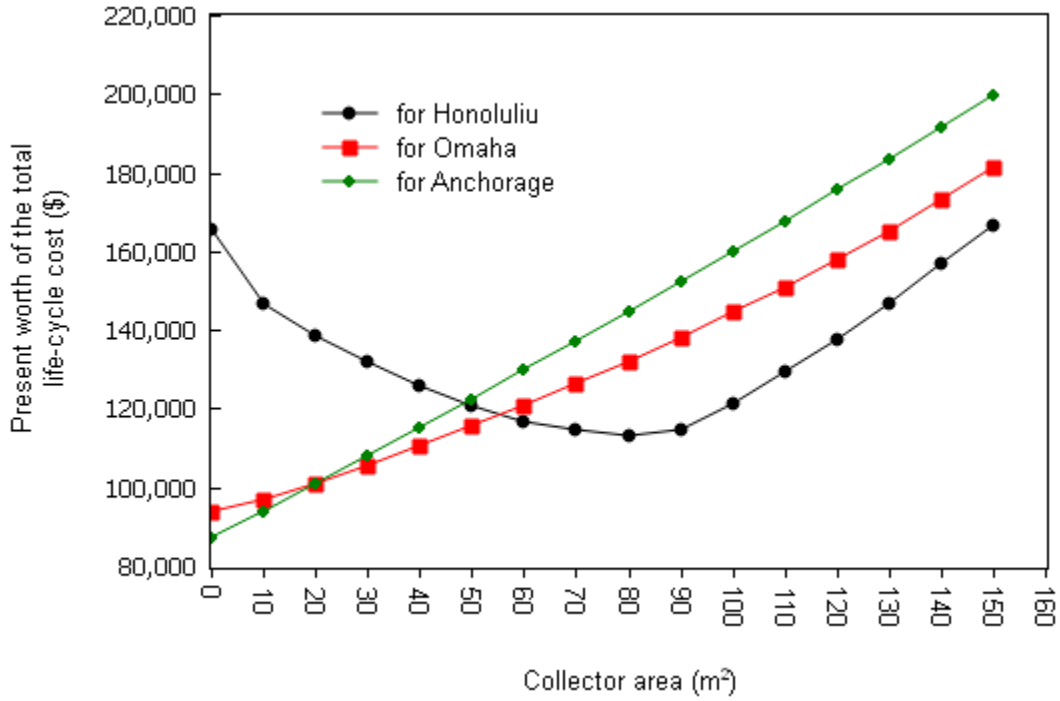

Figure 4.10: Effect of collector area on total life-cycle cost of a solar thermal energy system for three selected locations

A Summary of the economic analysis of the system described in Table 4.3 is presented in Table 4.5 below for all three locations. For the system with same collector area and pre-heating system size (same collector and pre-heating system cost), the total life-cycle cost is largest for Anchorage, followed by Omaha and Anchorage, respectively. As would be expected, the annual savings are also largest for Honolulu, followed by Omaha and Anchorage.

Table 4.5: Solar-gas heating system savings summary (collector area of 70 m^2)

Description	Honolulu	Omaha	Anchorage
Collector installation cost	$57,500	$57,500	$57,500
Pre-heating system installation cost	$13,500	$13,500	$13,500
Gas heater installation cost	$6,360	$17,600	$24,715
Present value of total life cycle cost	$114,335	$126,290	$137,215
Annual operation cost of the system*	$2,450	$2,495	$2,750
Annual cost savings	$6,305	$1,505	$810
CO_2e savings (tons/year)	15.73	10.01	6.39
Savings-to-investment ratio	0.74	0.17	0.09

Simple payback (years)**	12.27	59.02	118.21

*Annual operation cost is the sum of collector operation cost and gas heater operation cost.
**Annual operation cost of solar collectors is not considered in calculation of simple payback.

The minimum total life-cycle cost approach is useful in helping industry practitioners dimension the collector size based on the present worth of the total life-cycle cost. A similar analysis can be done to dimension the collector size based on the highest SIR value or lowest payback period.

4.5.4.2. Incentives Analysis

According to the U.S. Consolidated Appropriations Act [105], industrial solar energy projects that are installed by 2019 are eligible for a 30% federal investment tax credit (ITC) on the total investment [106]. This credit rate declines in subsequent years (e.g., 26% in 2020 and 22% in 2021). Beyond 2021, a 10% credit is scheduled for commercial and utility systems [106]. The total life-cycle cost of the solar flat-plate collector water heating system using climate data for Honolulu was recalculated after discounting the 30% ITC and is shown in Figure 4.11. It is seen that after applying ITC incentives, the minimum total life-cycle cost was obtained for a collector area value of 90 m^2 (solar fraction of 95.5%) instead of collector area of 80 m^2. A larger collector area indicates larger solar fraction and hence, less use of natural gas for auxiliary heating. Annual energy savings for this increased collector area was found to be $7,265. The corresponding SIR value was found to be 1.17, which indicates an economically viable investment. Similarly, the payback period (for a collector area of 90 m^2 after discounting incentives) was found to be 8.63 years.

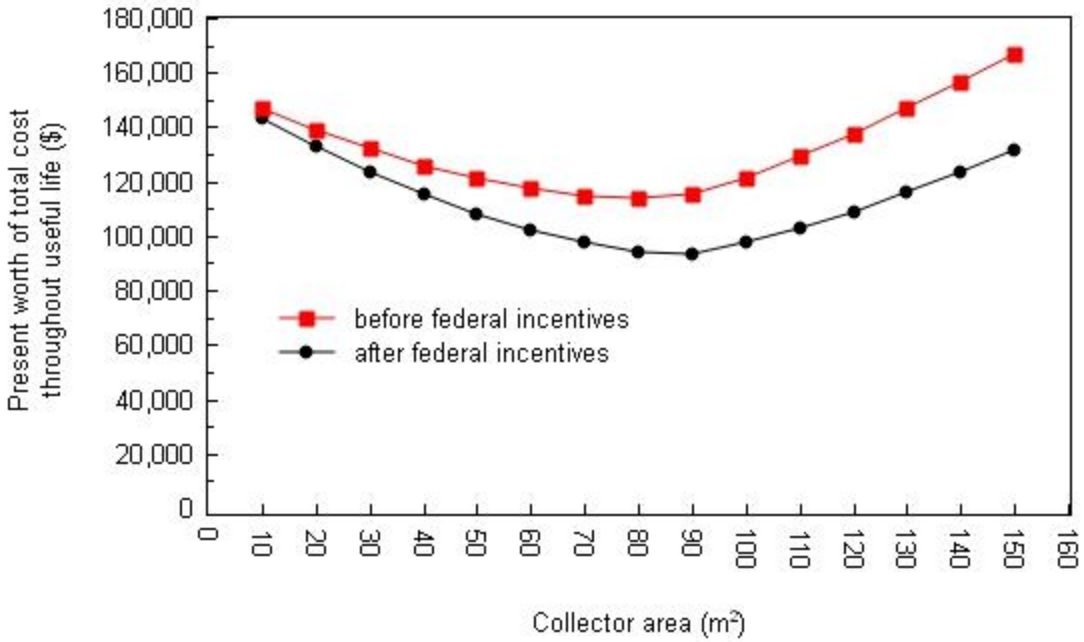

Figure 4.11: Total life-cycle cost before and after federal incentives using climate data for Honolulu

The economic performance indicators presented in Table 4.5 were recalculated after discounting for ITC incentives and are presented in Table 4.6. It can be seen, although the ITC incentives improved the SIR for all locations (32.4% increase for Honolulu, 23.5 % increase for Omaha, and 11.1% increase for Anchorage), it still not sufficient to justify the investment (as a SIR greater than 1 is considered worthy of economic investment). Several factors, such as collector-area dependent cost and price of natural gas contribute to this low SIR value; these effects are explored in the following section. Similarly, although the payback period was reduced by 11.5 years for Omaha and by 21.3 years for Anchorage, it is still too long to justify the investment; as the useful life of the system is assumed to be 25 years.

Table 4.6: Savings summary after applying ITC incentives (collector area of 70 m^2)

Description	Honolulu	Omaha	Anchorage
Present value of total life cycle cost	$97,085	$109,240	$119,965
Savings to investment ratio	0.98	0.21	0.10
Simple payback (years)*	9.53	47.53	96.9

*Annual operation cost of solar collectors is not considered in calculation of simple payback.

4.5.4.3. Sensitivity Analysis

A sensitivity analysis is performed to determine how the values of dependent variables change due to changes in independent variables. The one-factor-at-a-time (OFAT) [107] sensitivity analysis method is applied, where all input parameters are held constant except for one, which is varied using pre-determined low and high parameter values to evaluate the change in the model output values. The SIR of the solar flat-plate water heating system described in Table 4.3 is calculated and reported in Figure 4.12 for the following factors: natural gas cost rate, auxiliary gas heater cost per kW rating, collector area-dependent cost, heat exchanger cost per unit area, and discount rate. All input parameters were changed ±30% from the base case mentioned in Table 4.4. Similar to the above, the analysis was performed using climate data for Honolulu using a collector area of 90 m^2. The installation cost of solar collectors was calculated after discounting 30% ITC.

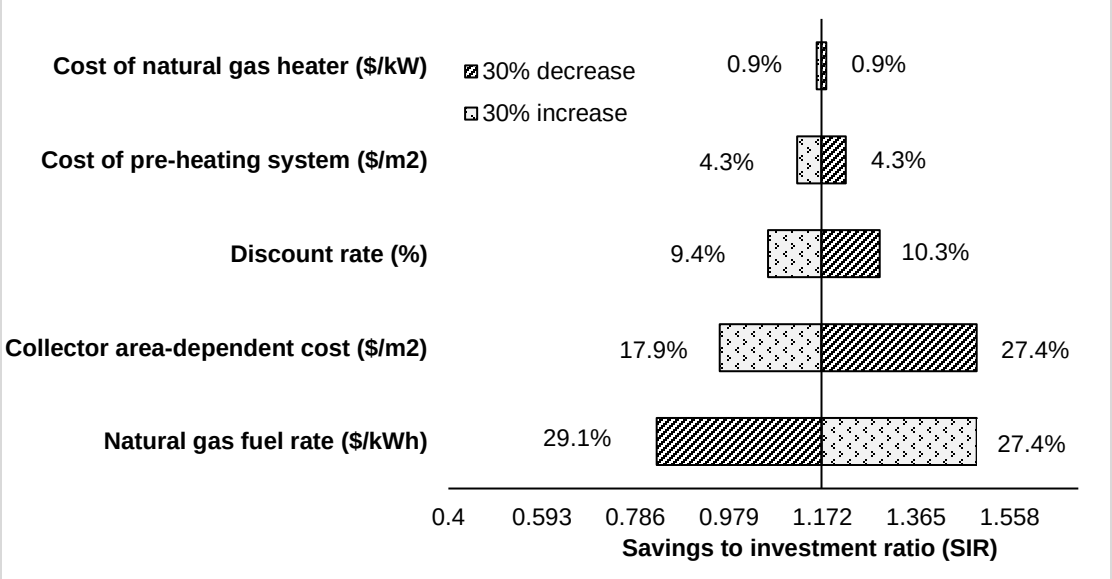

Figure 4.12: Sensitivity of the savings to investment ratio to different cost variables

It can be seen that SIR is most sensitive to natural gas cost followed by collector area-dependent cost, discount rate, pre-heating system cost, and auxiliary gas heater cost, respectively. As shown in Eq. 4.55, one of the most critical factors that directly affect the SIR value is the cost savings offered by solar flat-plate collectors. This cost savings value is calculated by comparing the solar-flat plate collector system with a gas-fired heating system, which is directly impacted by the natural gas fuel rate. Hence, the SIR

is most sensitive to the natural gas fuel price. Similarly, the solar flat-plate collectors followed by the pre-heating system and natural gas heater contribute the largest fraction of initial installation cost. Hence, the SIR is more sensitive to collector area-dependent cost followed by cost of pre-heating system and cost of natural gas heater. This analysis can help industry practitioners assess the economic feasibility of solar flat-plate collector water heating systems based on the SIR ratio. Additionally, the sensitivity analysis can be used to understand the uncertainties associated with the input variables and incorporate those uncertainties in the decision making process.

4.6. Conclusions

A review of existing literature shows that there is a dearth of simplified decision support tool to support small and medium sized manufacturing to assess the technical and economic feasibility of solar flat-plate collector energy systems in their businesses. Most of the available feasibility assessment methodologies are simulation-based that are expensive and require higher computation speed and technical knowledge to operate. Moreover, such methodologies often in their cost and energy calculation model do not consider the possibility of waste heat recovery that exists in an industrial facility. To contribute in filling this research gap, a feasibility assessment methodology was presented in this paper.

The $\bar{\phi}, f$-chart method and modified $\bar{\phi}, f$-chart design method were used to predict the amount of energy collected by the solar collectors. To assess the economic feasibility of solar flat-plate collector energy systems, a simplified cost model was presented, where the total cost of solar flat-plate collector energy system is expressed as sum of three major components: flat-plate collectors, auxiliary gas heater, and pre-heating system. The methodology was demonstrated using a decision support tool developed in MS Excel by exploring several what-if scenarios and performing a sensitivity analysis.

The solar fraction achieved by a typical solar flat-plate collector water heating system was calculated for different climate regions by considering eleven cities across the US. A maximum annual average solar fraction of 82.6% was obtained for Honolulu, HI, and minimum solar fraction of 33.6% was obtained for Anchorage, AK. Similarly, the

solar fractions for various collector sizes were calculated using climate data for Honolulu, Omaha, and Anchorage to explore the effect of increasing collector area on annual average solar fraction values.

The total life-cycle cost of a solar flat-plate collector water heating system was calculated for different collector area values using climate data for Honolulu, Omaha, and Anchorage. A minimum total cost was found for collector area of 80 m^2 for Honolulu. However, the minimum total cost for both Omaha and Anchorage was found for collector area of 0 m^2, which indicates that it is advantageous in terms of total life cycle cost to not install solar collectors. After discounting for federal incentives, a minimum total cost was found for a collector area of 90 m^2 Honolulu. The increased collector area resulted in an increase in annual average solar fraction and hence, reduction in annual average natural gas usage. A sensitivity analysis of savings-to-investment ratio (SIR) was performed by changing selected input parameters by ±30% from the base case. It was found that the SIR ratio was most sensitive to natural gas fuel rate followed by collector area dependent cost, discount rate, cost of pre-heating system, and cost of auxiliary gas heater. This suggests that locations with higher natural gas fuel rate are more suitable for application of solar flat-plate collector energy systems.

The MS Excel-based decision support tool is easy for practitioners to apply and requires less computational power compared to simulation-based tools. The scenario analysis presented within the tool can help industry practitioners identify whether solar flat-plate collectors would be adequate for energy collection with respect to their location and climate. Furthermore, the tool can be used to dimension the size of collectors based on the desired solar fraction. The cost calculation model presented within the tool can be easily manipulated to obtain a combination of solar flat-plate collectors, natural gas heating system, and preheating system with lowest possible total cost. Lastly, the sensitivity analysis presented in the tool can be performed to understand the uncertainties associated with the input variables.

4.7. Nomenclature

a	Coefficient defined in Equation 24
a^*	Coefficient defined in Equation 15
A_C	Collector area (m^2)
A_{HE}	Heat exchanger area (m^2)
b	Coefficient defined in Equation 25
b^*	Coefficient defined in Equation 26
c	Coefficient defined in Equation 15
C_A	Collector area-dependent cost ($\$ m^{-2}$)
C_f	Collector area-independent cost ($)
C_{FPC}	Cost of solar flat-plate collectors ($)
C_{GH}	Cost of auxiliary gas heating system ($)
C_H	Cost of auxiliary gas water heater per kW rating ($\$ kW^{-1}$)
C_{HE}	Cost of heat exchanger per unit area ($\$ m^{-2}$)
C_{GI}	Installation cost of gas water heater ($)
C_{HR}	Total cost of pre-heating system ($)
C_L	Coefficient defined in Equations 39 and 40
C_{min}	Minimum capacitance rate for a heat exchanger ($W\ °C^{-1}$)
$C_{O\&M}$	Collector operation and maintenance cost ($\$ year^{-1}$)
C_{OP}	Operating cost of auxiliary gas heating system ($\$ year^{-1}$)
c_p	Specific heat ($kJ\ kg^{-1}\ °C^{-1}$)
C_S	Cost savings ($\$ year^{-1}$)
C_{SI}	Initial system cost of solar flat-plate collectors ($)
$C_{S\text{-}life}$	Cost savings over useful life ($)
d	Discount rate (%)
$E_{without\ solar}$	Energy consumed by a natural gas water heating system with a pre-heating system ($kWh\ year^{-1}$)
$E_{with\ solar}$	Energy consumed by a solar flat-plate collector water heating system ($kWh\ year^{-1}$)

f	Solar fraction
F_R	Collector overall heat removal efficiency factor
g	Coefficient defined in Equation 42
G_{SC}	Solar constant
$\bar{H}$	Monthly average daily total solar radiation on a horizontal surface (J m^{-2})
$\overline{H_d}$	Monthly average daily diffuse radiation (J m^{-2})
$\overline{H_o}$	Monthly average daily extraterrestrial radiation (J m^{-2})
$\overline{H_t}$	Monthly average daily total solar radiation on the collector surface (J m^{-2})
I_{min}	Minimum critical radiation level (W)
$\overline{K_T}$	Ratio of monthly average total to the monthly average extraterrestrial radiation on a horizontal surface
L	Monthly heating load (J)
L_s	Useful load supplied by solar collectors (J)
M	Mass of liquid stored (kg)
N	Number of days in a month
n	Number of days in a year
NG_R	Price of natural gas (\$ kWh^{-1})
PW	Present worth (\$)
Q_{max}	Maximum total energy collection (J)
Q_{st}	Storage tank monthly energy losses (J)
q_{useful}	Rate of useful energy (W)
$\bar{R}$	Ratio of monthly average daily total radiation on a tilted surface to that on a horizontal surface
$\overline{R_b}$	Ratio of average daily beam radiation on a tilted surface to that on a horizontal surface
$R_{b,\,n}$	Ratio of beam radiation on a collector surface to that on a horizontal surface for the noon hour

$r_{d,\,n}$	Ratio of diffuse solar radiation at noon to the total solar daily radiation for the month central day
R_n	Ratio of radiation on a tilted surface to that on a horizontal surface at noon
R_s	Ratio of standard storage heat capacity per unit of collector area to the actual storage capacity per unit of collector area
$r_{t,\,n}$	Ratio of radiation at noon to the daily total radiation
SIR	Savings to investment ratio
S_{GH}	Gas water heater energy rating (kW)
T_a	Monthly average ambient temperature (°C)
T_{env}	Monthly average ambient temperature at the location of the storage tank (°C)
T_i	Fluid inlet temperature for the collector (°C)
T_{mains}	Temperature of make-up water (°C)
T_{min}	Minimum useful fluid temperature for a target process (°C)
$\overline{T_s}$	Monthly average storage tank temperature (°C)
t_o	Annual operating days
T'_{min}	Temperature necessary to meet a fraction *f* of the average load rate (°C)
TC	Total cost ($)
TC_{life}	Total life-cycle cost ($)
Δt	Number of hours in a month
U_L	Collector overall heat loss coefficient (W m^{-2} $°C^{-1}$)
$(UA)_a$	Auxiliary tank conductance for heat loss (W $°C^{-1}$)
$(UA)_t$	Pre-heat tank conductance for heat loss (W $°C^{-1}$)
X	Dimensionless variable defined in Equation 29
$\overline{X_{c,min}}$	Minimum monthly average critical radiation ratio
Y	Dimensionless variable defined in Equation 27
Z	Dimensionless variable defined in Equation 38

Greek

α	Absorptance
τ	Transmittance
$\overline{(\tau\alpha)}$	Monthly average energy weighted transmittance-absorptance product
$(\tau\,\alpha)_n$	Transmittance-absorptance product for radiation at normal incidence
$\overline{\phi_{max}}$	Maximum monthly average daily collector utilizability
δ	Declination
ω_s	Sunset hour angle (degrees)
Φ	Latitude (degrees)
β	Collector tilt angle (degrees)
γ	Surface azimuth angle (degrees)
ρ_g	Ground reflectance
$\bar{\phi}$	Monthly average daily utilizability
ε_L	Effectiveness of load heat exchanger
η_H	Efficiency of gas water heater (%)

Chapter 5. Conclusions

5.1. Summary

The improvement of collector technology in recent years has made solar thermal energy systems a cost effective alternative for low temperature process heat generation. Yet, there is a low adoption of solar thermal energy technologies in US manufacturing industries. Business owners will want to invest on solar thermal technologies if they see a clear economic benefit after performing site-specific feasibility studies. However, the cost and demand of technical resources required to conduct the feasibility study itself has made business owners reluctant towards analyzing the possibility of solar thermal energy systems. There is a lack of readily available cost-effective design decision support tools that can be used by industry analysts to appraise the merits of solar thermal energy systems. This research was undertaken with a goal of lowering the barrier for deployment of solar thermal energy systems for industrial process heating applications. The following tasks were undertaken as a part of this research.

Task 1: A set of designed experiments of a solar/gas hybrid domestic water heating system was performed under different modes of heating, temperature lifts, and solar insolation values. Using the collected data, the following performance metrics were calculated: solar collector efficiency, gas-fired heater efficiency, and solar/gas combined system efficiency. Results of the experimental study was used to identify a system configuration that would provide higher overall system efficiency when operating the hybrid system in combined solar/gas heating mode.

Task 2: A design decision support tool to assist industry analysts in evaluating the feasibility of solar flat-plate collector energy systems for industrial process heating was developed and presented in this research. To support the economic analysis, a cost model was developed and presented. A sensitivity analysis was presented to quantify the uncertainties associated with the input parameters. The use of the decision support tool along with the analysis of several what-if scenarios was demonstrated through an example application.

5.2. Conclusions

The experimental study of solar/gas hybrid water heating system under different temperature lift and solar inputs provided insight on the operational characteristics of hybrid systems. Moreover, the experimental study provided an understanding of which process heating loads might be best served with solar/gas hybrid system based on site insolation and gas prices, providing a basis for developing performance and cost prediction methodologies. When operating the hybrid system in a combined solar and gas heating mode, it was found that the energy consumed by the gas fired heater per degree temperature rise of process fluid increased with increase in solar input, suggesting that the hybrid system is less efficient in combined heating mode. This enabled the understanding of how the hybrid system behaves when operating in a combined solar and gas mode, while providing opportunities to identify system configurations with higher efficiencies.

The use and development of design decision support tool presented in Chapter 4 of this thesis enabled the analysis of several what-if scenarios under which solar thermal systems can be feasible. The performance comparison of solar thermal systems at different locations and climate regions presented within the tool provided the understanding of how energy collected by solar collectors varies with solar radiation values as well as helped in the identification of locations that are suitable for application of solar thermal energy systems. The sensitivity analysis presented within the tool showed that the savings to investment ratio (SIR) is most sensitive to natural gas fuel rate, suggesting that locations with higher natural gas prices are more suitable for application of solar thermal systems. The cost calculation model presented within the tool enabled the identification of a combination of solar flat-plate collectors, natural gas heating system, and preheating system with lowest total life-cycle cost.

5.3. Contributions

Presented work has made several contributions to the industrial and academic research community as described below.

Contribution 1: Experimental data on the thermal performance of solar/gas hybrid water heating system is presented in Chapter 3 of this thesis. Results of the experimental study serve as a benchmark for future experiment-based studies and can be used to identify potential areas of opportunity for improving design of solar/gas hybrid water heating systems. A system configuration that would provide higher overall system efficiency when running the solar/gas hybrid system in combined solar and gas heating mode was proposed in Chapter 3. This proposed system configuration offers natural gas energy savings when the solar/gas hybrid water heating system is operating at low and mid-range (15 to 50%) solar fraction, while enabling an easier and more accurate prediction of the actual energy and cost savings offered by hybrid system under various design conditions. The proposed configuration can be used as a design benchmark for conducting feasibility assessment of solar/gas hybrid water heating systems.

Contribution 2: A design decision support tool for feasibility assessment of solar thermal energy systems for industrial process heating was presented in Chapter 4 of this thesis. The design decision support tool enables small and medium sized enterprise to design and appraise the merits of solar thermal energy system in their business. The performance estimation and cost calculation model presented within the decision support tool can be used by enterprises to analyze various what-if scenarios under which solar thermal systems might be cost-effective. The sensitivity analysis presented within the tool can be used to quantify uncertainties associated the input variables and understand their implications in the decision. The cost model presented in the tool can be used to identify a system design with minimum life-cycle cost.

5.4. Opportunities for Future Research

The following opportunities for future research that have been identified as a direct result of this research:

Opportunity 1: Experimental study of the solar/gas hybrid water heating system presented in Chapter 3 of this thesis is based on limited climate data (Summer 2017 in Corvallis, Oregon). To accurately predict the annual performance of such hybrid systems, year-round experimental studies should be performed under different weather

conditions. This can be accomplished by: 1) monitoring the performance of the system every day for one full year, and 2) calculating the performance metrics using the collected data.

Opportunity 2: The feasibility assessment methodologies presented in Chapter 4 require manual observations of total life-cycle cost graphs to identify system designs with minimum life cycle cost. The graphs are plotted using data points at fixed intervals (multiples of 10). Hence, the system design obtained is only "close to optimal." Furthermore, only one criterion (total life cycle cost) is used to dimension the system. Future studies can consider multi-criteria (minimize total life cycle cost and maximize life-cycle savings) optimization approaches to identify optimal system designs. To perform design optimization, detailed mathematical models of the objective function and constraints need to be developed first. Then after, the next step would be to develop algorithms to solve the mathematical models.

Opportunity 3: The feasibility assessment methodology presented in Chapter 4 is limited to solar flat-plate collectors, which are limited to low temperature (<100 °C) heating applications. A large fraction (27%) of industrial process heating applications require temperature in the range of 100 to 400 °C which can be easily met by medium and high temperature solar collectors, such as evacuated tube collectors (ETCs) and concentrating solar power (CSP) collectors. Future work can expand and present feasibility assessment methodologies for ETCs and CSP collectors. This can be accomplished by: 1) reviewing existing solar thermal performance prediction models in the literature and identifying appropriate models for ETCs and CSP collectors, 2) developing appropriate cost calculation models, 3) documenting thermal performance prediction and cost calculation model in spreadsheet platforms, and 4) validating the models by comparing the results with the results of simulation based software.

References

[1] J. Veerapen, M. Beerepoot, Co-generation and Renewables, IEA Paris. (2011).

[2] S. Mekhilef, R. Saidur, A. Safari, A review on solar energy use in industries, Renew. Sustain. Energy Rev. 15 (2011) 1777–1790.

[3] M. Höök, X. Tang, Depletion of fossil fuels and anthropogenic climate change—A review, Energy Policy. 52 (2013) 797–809.

[4] O. Edenhofer, R. Pichs-Madruga, Y. Sokona, K. Seyboth, P. Matschoss, S. Kadner, T. Zwickel, P. Eickemeier, G. Hansen, S. Schlömer, IPCC special report on renewable energy sources and climate change mitigation, Prep. Work. Group III Intergov. Panel Clim. Change Camb. Univ. Press Camb. UK. (2011).

[5] P. Horta, I.S.E. FhG, Process Heat Collectors: State of the Art and available medium temperature collectors, SolarPaces Annex IV IEA SHC Task. 49 (2015).

[6] P. Lorenz, D. Pinner, T. Seitz, The Economics of Solar Power, Mckinsey Q. 4. (2008) 66–74.

[7] Renewable Energy and Jobs – Annual Review 2017, International Renewable Energy Agency, 2017. http://www.irena.org/documentdownloads/publications/irena_re_jobs_annual_review_2017.pdf.

[8] W. Weiss, M. Spörk-Dür, F. Mauthner, Global Market Development and Trends in 2016, IEA Solar Heating & Cooling Programme, 2017.

[9] J.H. Davidson, Low-temperature solar thermal systems: An untapped energy resource in the United States, J. Sol. Energy Eng. 127 (2005) 305–306.

[10] S. Kalogirou, The potential of solar industrial process heat applications, Appl. Energy. 76 (2003) 337–361.

[11] H. Schweiger, J.F. Mendes, N. Benz, K. Hennecke, G. Prieto, M. Cusí, H. Gonçalves, The potential of solar heat in industrial processes. A state of the art review for Spain and Portugal, in: EuroSun, 2000.

[12] K. Hennecke, Solar Process Heat for Production and Advanced Applications, IEA SHC Task, 49 (2015).

[13] H.P. Garg, Advances in Solar Energy Technology: Volume 3 Heating, Agricultural and Photovoltaic Applications of Solar Energy, Springer Science & Business Media, 2012.

[14] A. Aidonis, V. Drosou, T. Mueller, L. Staudacher, F. Fernandez-Llebrez, A. Oikonomou, S. Spencer, PROCESOL II-Solar thermal plants in industrial processes: Design and Maintenance Guidelines, Cent. Renew. Energy Sources Pikermi Greece. (2002).

[15] C. Vannoni, R. Battisti, S. Drigo, Potential for solar heat in industrial processes, 2008.

[16] R. Kempener, Solar Heat for Industrial Processes-Technology Brief, IRENA, 2015. https://www.solarthermalworld.org/sites/gstec/files/news/file/2015-02-27/irena-solar-heat-for-industrial-processes_2015.pdf.

[17] M. Atkinson, Improving Process Heating System Performance: A Sourcebook for Industry, U.S. Department of Energy, Energy Efficiency and Renewable Energy, 2004. https://www.nrel.gov/docs/fy04osti/35992.pdf.
[18] Monthly Energy Review – March 2018, U.S. Energy Information Administration, 2018. https://www.eia.gov/totalenergy/data/monthly/pdf/mer.pdf.
[19] B.M. Fronk, C.M. Keinath, Comparison of Primary Energy Consumption of Vapor and Non-Vapor Compression Natural Refrigerant Heat Pumps for Domestic Hot Water Applications, in: 12th IEA Heat Pump Conf. 2017, 2017.
[20] J.B. Maguire, A parametric analysis of residential water heaters, University of Colorado at Boulder, 2012.
[21] D. Makaire, P. Ngendakumana, Thermal performance of condensing boilers, (2010).
[22] M. Cotrado, A. Dalibard, R. Söll, D. Pietruschka, Design, control and first monitoring data of a large scale solar plant at the Meat Factory Berger, Austria, Energy Procedia. 48 (2014) 1144–1151.
[23] C. El Mkadmi, A. Wahed, Optimization of a solar thermal system for low temperature industrial heating process, in: Renew. Sustain. Energy Conf. IRSEC 2016 Int., IEEE, 2016: pp. 313–319.
[24] N. Benz, M. Gut, T. Beikircher, Solar process heat with non-concentrating collectors for food industry, in: Proc. ISES Sol. World Congr., 1999.
[25] H. Muller, Solar Process Heat in the Food Industry–Methodological Analysis and Design of a Sustainable Process Heat Supply System in a Brewery and a Dairy, (2016).
[26] J.A. Duffie, W.A. Beckman, Solar engineering of thermal processes, John Wiley & Sons, 2013.
[27] S.A. Kalogirou, Solar thermal collectors and applications, Prog. Energy Combust. Sci. 30 (2004) 231–295.
[28] R. American Society of Heating, A.-C. Engineers, 1996 ASHRAE Handbook: Heating, Ventilating, and Air-Conditioning Systems and Equipment, American Society of heating, refrigerating and air-conditioning engineers, Atlanta, Georgia, 1996.
[29] R. Shukla, K. Sumathy, P. Erickson, J. Gong, Recent advances in the solar water heating systems: A review, Renew. Sustain. Energy Rev. 19 (2013) 173–190.
[30] S.A. Kalogirou, Solar energy engineering: processes and systems, Academic Press, 2013.
[31] S.J.B. Hale, ANSI/ASHRAE Standard 93-2003, Methods of Testing to Determine the Thermal Performance of Solar collectors, (2003).
[32] CSN EN 12975-2 - Thermal solar systems and components - Solar collectors - Part 1: General requirements, (2006).
[33] K.R. Anderson, S. Hill, C. Selerberg, E. Guiterez, Experimental study of Sunearth flat plate solar collector, Int. J. Energy Eng. 4 (2014) 31.
[34] D. Rojas, J. Beermann, S.A. Klein, D.T. Reindl, Thermal performance testing of flat-plate collectors, Sol. Energy. 82 (2008) 746–757.

[35] E. Zambolin, D. Del Col, Experimental analysis of thermal performance of flat plate and evacuated tube solar collectors in stationary standard and daily conditions, Sol. Energy. 84 (2010) 1382–1396.
[36] T. Osório, M.J. Carvalho, Testing of solar thermal collectors under transient conditions, Sol. Energy. 104 (2014) 71–81.
[37] L.M. Ayompe, A. Duffy, Analysis of the thermal performance of a solar water heating system with flat plate collectors in a temperate climate, Appl. Therm. Eng. 58 (2013) 447–454.
[38] I.M. Michaelides, P.C. Eleftheriou, An experimental investigation of the performance boundaries of a solar water heating system, Exp. Therm. Fluid Sci. 35 (2011) 1002–1009.
[39] M.C. Rodriguez-Hidalgo, P.A. Rodríguez-Aumente, A. Lecuona, J. Nogueira, Instantaneous performance of solar collectors for domestic hot water, heating and cooling applications, Energy Build. 45 (2012) 152–160.
[40] C. Vannoni, R. Battisti, S. Drigo, SHIP–Plant Survey Report, IEA SHC Task. 33 (2006).
[41] O. US EPA, Renewable Industrial Process Heat, US EPA. (2014). https://www.epa.gov/rhc/renewable-industrial-process-heat (accessed April 17, 2018).
[42] P. Kurup, C. Turchi, Potential for solar industrial process heat in the United States: A look at California, in: AIP Conf. Proc., AIP Publishing, 2016: p. 110001.
[43] Transient System Simulation Tool, University of Wisconsin, Madison, WI, n.d. http://www.trnsys.com/ (accessed February 23, 2018).
[44] N. Benz, M. Gut, W. Rub, Solar process heat in breweries and dairies, in: Proc. EuroSun, 1998: pp. 2–5.
[45] N. Eskin, Performance analysis of a solar process heat system, Energy Convers. Manag. 41 (2000) 1141–1154.
[46] Saving Energy with Electric Resistance Heating, NREL (National Renewable Energy Laboratory (NREL), Golden, CO (United States)), 1997. https://www.nrel.gov/docs/legosti/fy97/6987.pdf (accessed November 17, 2017).
[47] Residential Energy Consumption Survey (RECS) - Data - U.S. Energy Information Administration (EIA), (2015). https://www.eia.gov/consumption/residential/data/2015/ (accessed April 10, 2018).
[48] E.C. Balke, W.M. Healy, T. Ullah, An assessment of efficient water heating options for an all-electric single family residence in a mixed-humid climate, Energy Build. 133 (2016) 371–380.
[49] Energy Information Administration (EIA)- About the Residential Energy Consumption Survey (RECS)Table HC1.1 Fuels used and end uses in U.S. homes by housing unit type, 2015, (2015). https://www.eia.gov/consumption/residential/data/2015/hc/php/hc8.9.php (accessed November 12, 2017).
[50] M.C. Rodríguez-Hidalgo, P.A. Rodríguez-Aumente, A. Lecuona, G.L. Gutiérrez-Urueta, R. Ventas, Flat plate thermal solar collector efficiency:

Transient behavior under working conditions part II: Model application and design contributions, Appl. Therm. Eng. 31 (2011) 2385–2393.
[51] I.M. Michaelides, P.C. Eleftheriou, An experimental investigation of the performance boundaries of a solar water heating system, Exp. Therm. Fluid Sci. 35 (2011) 1002–1009.
[52] A. Handbook-Heating, 2016 ASHRAE Handbook: Ventilating, and Air-Conditioning Systems and Equipment (IP Edition), ASHRAE, Atlanta, GA 30329, 2016.
[53] J.B. Maguire, A parametric analysis of residential water heaters, PhD Thesis, University of Colorado at Boulder, 2012.
[54] R. Aldrich, Indirect Solar Water Heating in Single-Family, Zero Energy Ready Homes, NREL (National Renewable Energy Laboratory (NREL), Golden, CO (United States)), 2016.
[55] B.N. Taylor, C.E. Kuyatt, Guidelines for evaluating and expressing the uncertainty of NIST measurement results, US Department of Commerce, Technology Administration, National Institute of Standards and Technology Gaithersburg, MD, 1994.
[56] EES: Engineering Equation Solver | F-Chart Software : Engineering Software, (n.d.). http://www.fchart.com/ees/ (accessed November 28, 2017).
[57] S.A. Klein, W.A. Beckman, A general design method for closed-loop solar energy systems, Sol. Energy. 22 (1979) 269–282.
[58] Y. You, E.J. Hu, A medium-temperature solar thermal power system and its efficiency optimisation, Appl. Therm. Eng. 22 (2002) 357–364.
[59] R. Celuppi, J. Scapinello, F.G. Andrade, J.H. Revello, J.D. Magro, Solar energy use for water pre-heating in boilers of agro-industries, Eng. Agríc. 34 (2014) 451–460.
[60] R.G. Boundy, S.W. Diegel, L.L. Wright, S.C. Davis, Biomass Energy Data Book: Edition 4, Oak Ridge National Laboratory (ORNL), 2011.
[61] Dylan Cutler, Jesse Dean, Jason Acosta, Dennis Jones, Condensing Boilers Evaluation: Retrofit and New Construction Applications, (2014). https://www.gsa.gov/cdnstatic/Condensing_Boilers_2014a_%28508%29.pdf (accessed December 23, 2017).
[62] A. Handbook, Heating, Ventilating, and Air-Conditioning Applications. Atlanta: American Society of Heating, Refrigerating and Air-Conditioning Engineers, Inc, 2011.
[63] M.A. Hoeschele, D.A. Springer, Field and Laboratory Testing of Gas Tankless Water Heater Performance., ASHRAE Trans. 114 (2008).
[64] Bill Healy, Water Heating Technologies and Ratings, National Institute of Standards and Technology, 2015. https://www.nist.gov/sites/default/files/documents/iaao/Healy.pdf (accessed January 5, 2018).
[65] Tankless or Demand-Type Water Heaters | Department of Energy, Energy.Gov. (n.d.). https://energy.gov/energysaver/tankless-or-demand-type-water-heaters (accessed December 2, 2017).
[66] Static Sankey Diagram of Process Energy in U.S. Manufacturing Sector | Department of Energy, (2010). https://www.energy.gov/eere/amo/static-

sankey-diagram-process-energy-us-manufacturing-sector (accessed May 23, 2017).
[67] U.S. Energy Information Administration (EIA) - Data, (2017). https://www.eia.gov/consumption/data.php#mfg (accessed April 16, 2018).
[68] K. Kurokawa, Energy from the desert: practical proposals for very large scale photovoltaic systems, Earthscan, 2007.
[69] G.R. Timilsina, L. Kurdgelashvili, P.A. Narbel, Solar energy: Markets, economics and policies, Renew. Sustain. Energy Rev. 16 (2012) 449–465.
[70] U. Herrmann, B. Kelly, H. Price, Two-tank molten salt storage for parabolic trough solar power plants, Energy. 29 (2004) 883–893.
[71] C. Philibert, Barriers to technology diffusion: the case of solar thermal technologies, Int. Energy Agency Organ. Econ. Dev. (2006).
[72] H. Cassard, P. Denholm, S. Ong, Technical and economic performance of residential solar water heating in the United States, Renew. Sustain. Energy Rev. 15 (2011) 3789–3800.
[73] S. Jacobsson, A. Johnson, The diffusion of renewable energy technology: an analytical framework and key issues for research, Energy Policy. 28 (2000) 625–640.
[74] Carbon Tax, Carbon Tax Cent. (n.d.). https://www.carbontax.org/states/ (accessed February 18, 2018).
[75] Arizona: Solar Pre-heating for Sports Drinks, Glob. Sol. Therm. Energy Counc. (n.d.). http://www.solarthermalworld.org/content/arizona-solar-pre-heating-sports-drinks (accessed February 20, 2018).
[76] Steam and Cooling: no Problem for a Solar Thermal System, Glob. Sol. Therm. Energy Counc. (n.d.). http://www.solarthermalworld.org/content/steam-and-cooling-no-problem-solar-thermal-system (accessed February 20, 2018).
[77] S. Suman, M.K. Khan, M. Pathak, Performance enhancement of solar collectors—A review, Renew. Sustain. Energy Rev. 49 (2015) 192–210.
[78] H. Schnitzer, C. Brunner, G. Gwehenberger, Minimizing greenhouse gas emissions through the application of solar thermal energy in industrial processes, J. Clean. Prod. 15 (2007) 1271–1286.
[79] C. Lauterbach, S. Javid Rad, B. Schmitt, K. Vajen, Feasibility assessment of solar process heat applications, in: Sol. World Congr. Kassel, 2011.
[80] V. Mcleod, J. Annas, W. Stein, J. Hinkley, Application of solar process heat to the commercial & industrial sectors, Syd. Aust. (2005).
[81] J. Siegenthaler, Heating with Renewable Energy, Cengage Learning, 2016.
[82] Polysun Simulation Software, Pixelizer, Switzerland, 1992. http://www.velasolaris.com/english/home.html (accessed February 23, 2018).
[83] Thermal simulation software T*SOL, Valentin Software, Inc, Temecula, CA, 2015. https://www.valentin-software.com/en/products/solar-thermal/14/tsol (accessed February 26, 2018).
[84] H. Lahmidi, TRANSOL, France, 2004. https://aiguasol.coop/energy-software/transol-3-solar-thermal-energy/ (accessed February 23, 2018).
[85] J.E. Braun, S.A. Klein, K.A. Pearson, An improved design method for solar water heating systems, Sol. Energy. 31 (1983) 597–604.

[86] A. Handbook, Heating, Ventilating, and Air-Conditioning Applications (IP Edition), Atlanta. (2011) 136–138.
[87] S.A. Klein, Calculation of monthly average insolation on tilted surfaces, Sol. Energy. 19 (1977) 325–329.
[88] P.I. Cooper, The absorption of radiation in solar stills, Sol. Energy. 12 (1969) 333–346.
[89] B.Y. Liu, R.C. Jordan, The interrelationship and characteristic distribution of direct, diffuse and total solar radiation, Sol. Energy. 4 (1960) 1–19.
[90] B.Y. Liu, R.C. Jordan, Availability of solar energy for flat-plate solar heat collectors, Appl. Sol. Energy Heat. Cool. Build. ASHRAE Atlanta. (1977).
[91] D.G. Erbs, S.A. Klein, J.A. Duffie, Estimation of the diffuse radiation fraction for hourly, daily and monthly-average global radiation, Sol. Energy. 28 (1982) 293–302.
[92] M. Collares-Pereira, A. Rabl, The average distribution of solar radiation-correlations between diffuse and hemispherical and between daily and hourly insolation values, Sol. Energy. 22 (1979) 155–164.
[93] T. Karl, W.J. Koss, Regional and national monthly, seasonal, and annual temperature weighted by area, 1895-1983, (1984).
[94] NASA Surface meteorology and Solar Energy - Location, (n.d.). https://eosweb.larc.nasa.gov/cgi-bin/sse/grid.cgi?email=skip@larc.nasa.gov (accessed April 16, 2018).
[95] M. Jamil Ahmad, G. N Tiwari, Optimization of tilt angle for solar collector to receive maximum radiation, Open Renew. Energy J. 2 (2009).
[96] H.K. Elminir, A.E. Ghitas, F. El-Hussainy, R. Hamid, M.M. Beheary, K.M. Abdel-Moneim, Optimum solar flat-plate collector slope: case study for Helwan, Egypt, Energy Convers. Manag. 47 (2006) 624–637.
[97] Siting Your Solar Water Heating System | Department of Energy, (n.d.). https://www.energy.gov/energysaver/siting-your-solar-water-heating-system (accessed March 7, 2018).
[98] A. Şerban, N. Bărbuţă-Mişu, N. Ciucescu, S. Paraschiv, S. Paraschiv, Economic and Environmental Analysis of Investing in Solar Water Heating Systems, Sustainability. 8 (2016) 1286.
[99] D.M. Atia, F.H. Fahmy, N.M. Ahmed, H.T. Dorrah, Optimal sizing of a solar water heating system based on a genetic algorithm for an aquaculture system, Math. Comput. Model. 55 (2012) 1436–1449.
[100] A. Walker, Solar Water Heating, in: Denver, Colorado, 2012. https://www.nrel.gov/docs/fy13osti/56706.pdf.
[101] M.J. Mossman, RSMeans, in: RSMeans Mech. Cost Data, 39th ed., 2016: pp. 363–367.
[102] R. Hackl, S. Harvey, Identification, cost estimation and economic performance of common heat recovery systems for the chemical cluster in Stenungsund, Chalmers University of Technology, 2013.
[103] U. Policy, Guide to cost-benefit analysis of investment projects, The EU. (2008).

[104] C. Rockenbaugh, J. Dean, D. Lovullo, L. Lisell, G. Barker, E. Hanckock, P. Norton, High Performance Flat Plate Solar Thermal Collector Evaluation, National Renewable Energy Lab.(NREL), Golden, CO (United States), 2016.
[105] C. Dent, Text - H.R.2029 - 114th Congress (2015-2016): Consolidated Appropriations Act, 2016, (2015). https://www.congress.gov/bill/114th-congress/house-bill/2029/text (accessed April 16, 2018).
[106] Leveraging Federal Renewable Energy Tax Credits | Department of Energy, (2016). https://www.energy.gov/eere/slsc/downloads/leveraging-federal-renewable-energy-tax-credits (accessed April 5, 2018).
[107] A. Saltelli, K. Chan, E.M. Scott, Sensitivity analysis, Wiley New York, 2000.